Geophysical Journal International

Geophys. J. Int. (2017) **210,** 852–873
Advance Access publication 2017 May 16
GJI Seismology

doi: 10.1093/gji/ggx197

Historical tsunami earthquakes in the Southwest Pacific: an extension to $\Delta > 80°$ of the energy-to-moment parameter Θ

Emile A. Okal and Nooshin Saloor

Department of Earth & Planetary Sciences, Northwestern University, Evanston, IL 60208*, USA. E-mail: emile@earth.northwestern.edu*

Accepted 2017 May 8. Received 2017 May 1; in original form 2016 October 18

SUMMARY

We extend to distances beyond 80° the computation of the energy-to-moment slowness parameter Θ introduced by Newman and Okal, by defining a regional empirical correction based on recordings at distant stations for events otherwise routinely studied. In turn, this procedure allows the study of earthquakes in a similar source-station geometry, but for which the only available data are located beyond the original distance threshold, notably in the case of historical earthquakes predating the development of dense networks of short-period seismometers. This methodology is applied to the twin 1947 earthquakes off the Hikurangi coast of New Zealand for which we confirm slowness parameters characteristic of tsunami earthquakes. In addition, we identify as such the large aftershock of 1934 July 21 in the Santa Cruz Islands, which took place in the immediate vicinity of the more recent 2013 shock, which also qualifies as a tsunami earthquake. In that subduction zone, the systematic compilation of Θ for both recent and pre-digital events shows a diversity in slowness correlating with local tectonic regimes controlled by the subduction of fossil structures. Our methodology is also well adapted to the case of analogue records of large earthquakes for which short-period seismograms at conventional distances are often off-scale.

Key words: New Zealand; Pacific Ocean; Earthquake source observations; Tsunami warning.

1 INTRODUCTION

This paper examines quantitatively three historical 'tsunami earthquakes' in the Southwest Pacific. We recall that this class of events was defined by Kanamori (1972) as earthquakes whose tsunamis are significantly larger than expected from their seismic magnitudes, especially classical ones; charter examples included the famous 1896 Sanriku and 1946 Aleutian earthquakes. Such events obviously pose enormous challenges, since tsunami warning remains largely based on an assessment of the parent earthquake (e.g. Okal 2008). While several models have been proposed to explain the occurrence of tsunami earthquakes in various environments (Fukao 1979; Tanioka *et al*. 1997; Bilek & Lay 2002), the systematics of their occurrence at any given subduction zone remain elusive. In this context, and because tsunami earthquakes are relatively rare, it is crucial to investigate as quantitatively as possible those events predating the development of digital networks. In the present paper, we extend to distances $\Delta > 80°$ the computation of the Energy-to-Moment parameter Θ, introduced by Newman & Okal (1998) and used as a robust discriminant to characterize source slowness, notably during tsunami earthquakes.

Following the work of Boatwright & Choy (1986), Newman & Okal (1998) developed an estimate E^E of the seismic energy radiated by an earthquake into its teleseismic body waves, not requiring the precise knowledge of focal mechanism and source depth (assuming the earthquake remains shallower than 80 km), and defined a slowness parameter:

$$\Theta = \log_{10} \frac{E^E}{M_0}, \tag{1}$$

where M_0 is the seismic moment of the source. Under seismic scaling laws, Θ should remain constant, its theoretical value being -4.90, but earthquakes featuring an anomalous source spectrum can have excessive or deficient Θ values, by as much as 2 logarithmic units, the latter being the case of tsunami earthquakes. In their original study, Newman & Okal (1998) had shown that three tsunami earthquakes (Nicaragua, 1992; Java, 1994; and Chimbote, Peru, 1996) postdating Kanamori's (1972) study all featured deficient values of Θ, in the -5.8 to -6.3 range. The computation of Θ was later implemented as part of routine procedures at a number of tsunami warning centres (e.g. Weinstein & Okal 2005).

In order to allow a proper, theoretically justifiable, implementation of a distance correction into the Θ algorithm, Newman & Okal (1998) originally restricted its use to the window $25° < \Delta < 90°$. In later studies (e.g. Okal & Newman 2001; Weinstein & Okal 2005; Okal 2013), we used a narrower range of distances ($35° < \Delta < 80°$), made possible by the abundance of digital stations deployed in recent years. At shorter distances, this guards against the effects of the triplications resulting from mantle discontinuities, and at greater ones, against complexities due to reflections such as *PcP*, and more

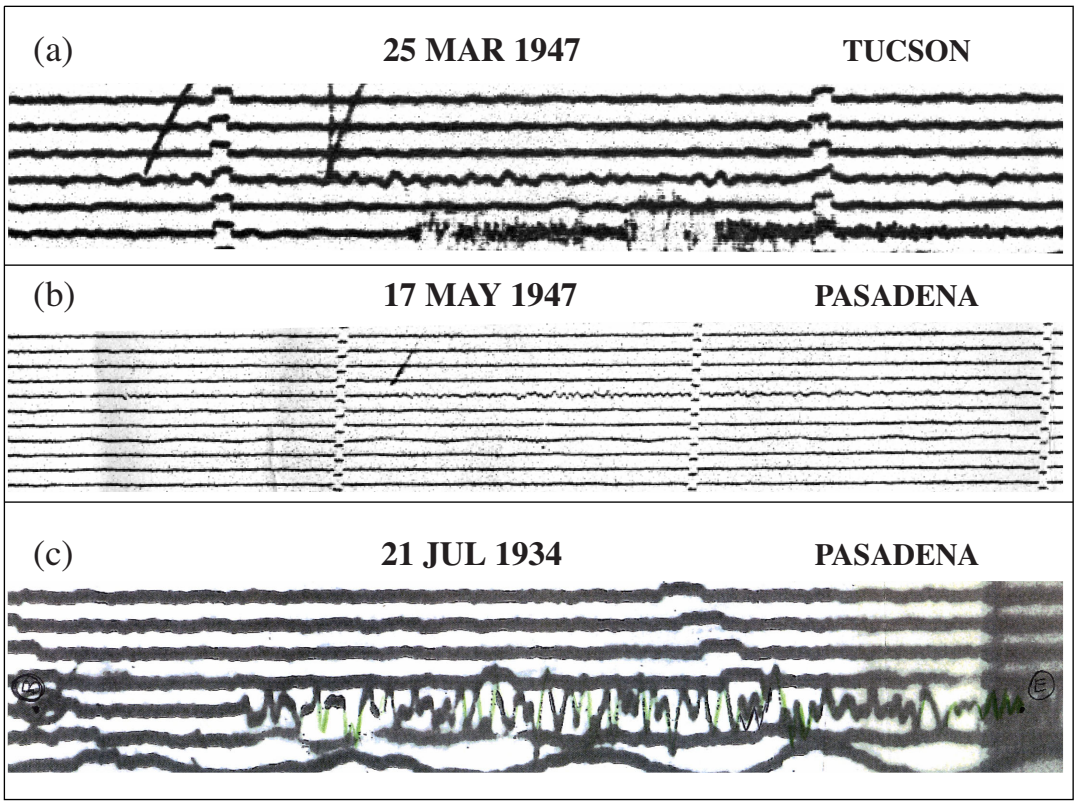

Figure 1. Short-period *P*-wave seismograms used in this study. Time marks are minutes, uncorrected for clock errors. The durations of the seismograms are 106 s (a), 179 s (b), and 90 s (c). On (a), the high-frequency signal recorded half-an-hour later is a local shock, unrelated to the New Zealand earthquake.

generally to the interaction of the generalized *P* wave with the *D″* boundary layer, known to feature considerable lateral heterogeneity (e.g. Garnero & Helmberger 1996), even before the initiation of genuine diffraction by the core–mantle boundary around 102°. In a previous contribution, Ebeling & Okal (2012) used large digital data sets to define an empirical correction allowing the extension of Θ to distances as short as 5°; in the context of tsunami warning in the regional field, these authors were motivated by the desire to obtain information on potential source slowness as soon as possible following the event, and hence from stations located as close as possible to the source.

Our motivation in the present paper is different. We have shown in a number of previous studies that the Θ concept can be successfully applied to historical events, helping define or confirm the anomalous behaviour of both slow tsunami earthquakes such as the Mexican aftershock of 1932 June 22 ($\Theta = -6.18$) and the Aleutian event of 1946 April 1 ($\Theta = -7.03$) (López & Okal 2006; Okal & Borrero 2011), and fast, 'snappy' events, such as the Chillán shock of 1939 January 25 ($\Theta = -4.04$) and the great Showa Sanriku earthquake of 1933 March 2 ($\Theta = -4.24$) (Okal & Kirby 2002; Okal *et al*. 2016). However, such investigations must rely on short-period records of body-wave arrivals offering adequate and documented response in the relevant frequency range (typically 0.1 to 2 Hz). While torsion seismometers (Anderson & Wood 1925) can occasionally provide adequate records for historical events, those instruments were typically low-gain, and they were deployed only in a few active areas such as Southern California, restricting their use to relatively short distances (e.g. 19° at PAS, for the 1932 Mexican earthquakes, Okal & Borrero 2011).

In the specific cases of the 1947 New Zealand and 1934 Santa Cruz earthquakes detailed below, it was not possible to find appropriate short-period records allowing quantification of body-wave energy at distances less than 80°, even though short-period instruments (Benioff 1932) were by then deployed at greater distances, either as prototypes (1934; Pasadena) or in regular operation (1947; Pasadena, Tucson). This study derives a methodology to quantify the information contained in those seismograms, reproduced on Fig. 1.

In addition, and as will be discussed in Section 5, the extension of the algorithm beyond 80° allows the occasional processing of large earthquakes from the era of the World-Wide Standardized Seismic Network (WWSSN), for which records at conventional distances may have gone off-scale.

2 THE 1947 HIKURANGI DOUBLET

The Eastern coast of the North Island of New Zealand, fringed by the Hikurangi Trench, was the site of two exceptional earthquakes on 1947 March 25 and May 17 (hereafter Events I and II, respectively). Their local magnitudes did not exceed $M_L = 5.9$ and 5.6, respectively, while their conventional surface magnitudes were $M_s = 7.2$ for both events (Bell *et al*. 2014). They were followed by local tsunamis running up 10 m and 6 m, respectively (Solov'ev & Go 1984a). Eiby (1947) has documented that Event I was hardly if at all felt (maximum MMI IV) in areas which were to be devastated 30 min later by the tsunami, while Event II was felt at maximum MMI of V. These properties clearly classify the two 1947 events as tsunami earthquakes.

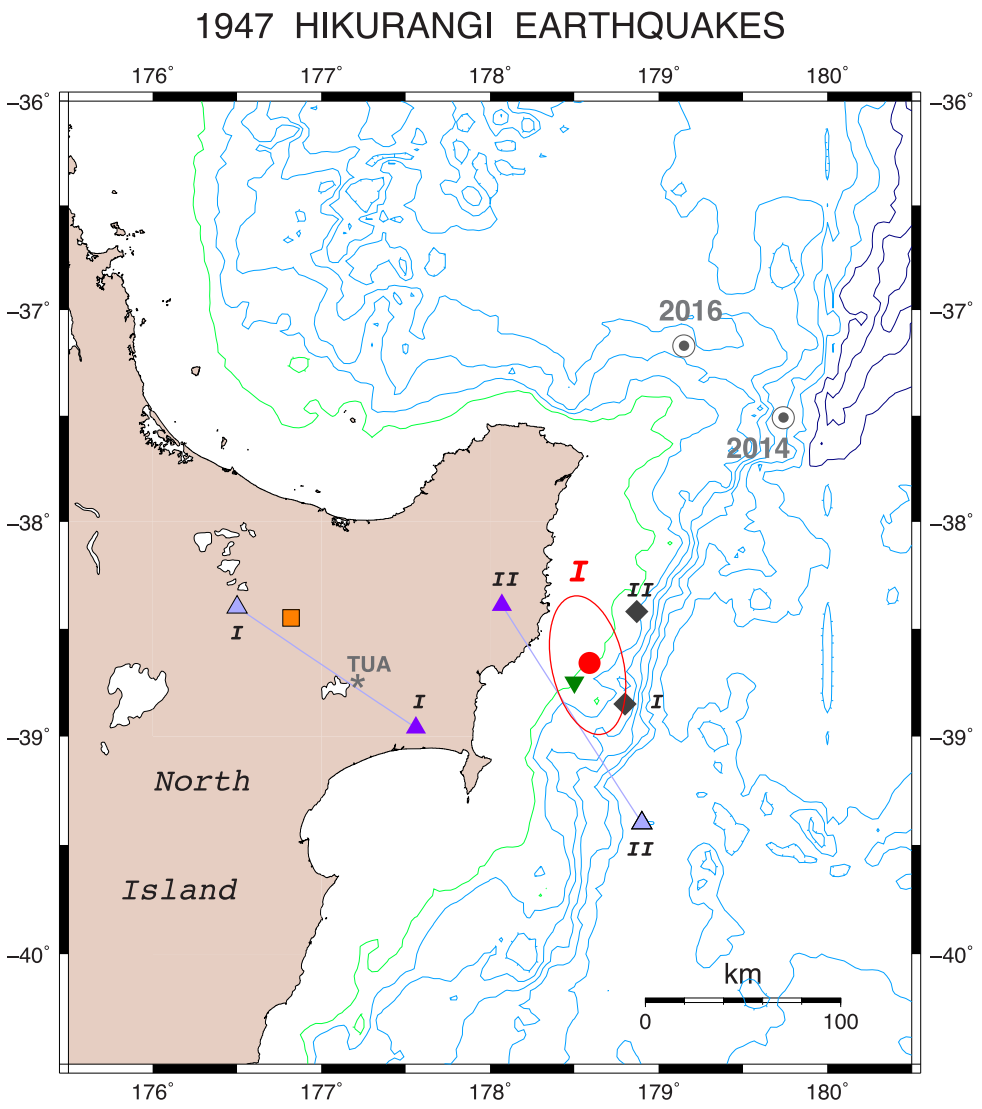

Figure 2. Relocations of the 1947 Hikurangi Events I and II. The red dot (with Monte Carlo ellipse) is our relocation of Event I (25 March), the green inverted triangle Gutenberg & Richter's (1954) epicentre, the light grey triangle the original ISS location, linked to the purple triangle showing the ISC-GEM solution; the orange square is the Centennial location (Engdahl & Villaseñor 2002), and the black diamond Downes *et al.*'s (2001). For Event II (17 May), the only locations available are the ISS (shaded triangle) and ISC-GEM (purple triangle), and Downes *et al.*'s (2001) (diamond). The asterisk shows the location of the incriminating station Tuai (TUA). The normal faulting validation events of 2014 and 2016 are shown as bull's eye symbols. Isobaths are at 500 m intervals (green at 500 m; dark blue at 4000 m and deeper).

The 1947 Hikurangi earthquakes were particularly poorly located by global agencies, including during modern relocation efforts such as the Centennial and ISC−GEM projects (Engdahl & Villaseñor 2002; Storchak *et al.* 2013). As shown on Fig. 2, the original ISS source for Event I, as well as its two modern estimates, locate as much as 150 km inside the North Island, and were assigned clearly erroneous depths of about 160 km. The ISS location for Event II, originally on the outer rise oceanwards of the trench, was moved onland during the ISC−GEM relocation, this supposedly improved epicentre being incompatible with the primary source of a large tsunami. We were able to relocate Event I at 38.66°S, 178.59°E, from phase data listed in the ISS, but excluding times at the nearby station Tuai (TUA; see below), using Wysession *et al.*'s (1991) algorithm which includes a Monte Carlo estimate for confidence ellipses obtained by injecting into the data set Gaussian noise (with a standard deviation $\sigma_G = 3$ s for events in the 1940s). A similar effort for Event II could not converge satisfactorily; that event is also absent from B. Gutenberg's notepads (Goodstein *et al.* 1980) and from the Centennial catalogue. As detailed by Downes *et al.* (2001), this unparalleled scattering of relocations, and especially the failure of global modern techniques, reflect the emergent character of arrivals, poorly correlated between stations, itself due to the slowness of the earthquake source. However, careful relocations by these authors, including a reappraisal of arrival times on original seismograms at New Zealand stations, led them to hypothesize that the closest station (TUA) may have recorded weak foreshocks; once the TUA times were removed, Downes *et al.* (2001) obtained solutions on the plate boundary in the immediate vicinity of the trench, at 38.85°S, 178.80°E for Event I, and 38.42°S, 178.87° E for Event II. These are shown as diamonds on Fig. 2, and will be used in this study. Note that our confidence ellipse for Event I grazes their solution; it is also remarkable that Gutenberg and Richter's (1954) epicentre, rounded to the nearest quarter-degree, fits inside our ellipse, a mere 28 km away from Downes *et al.* (2001).

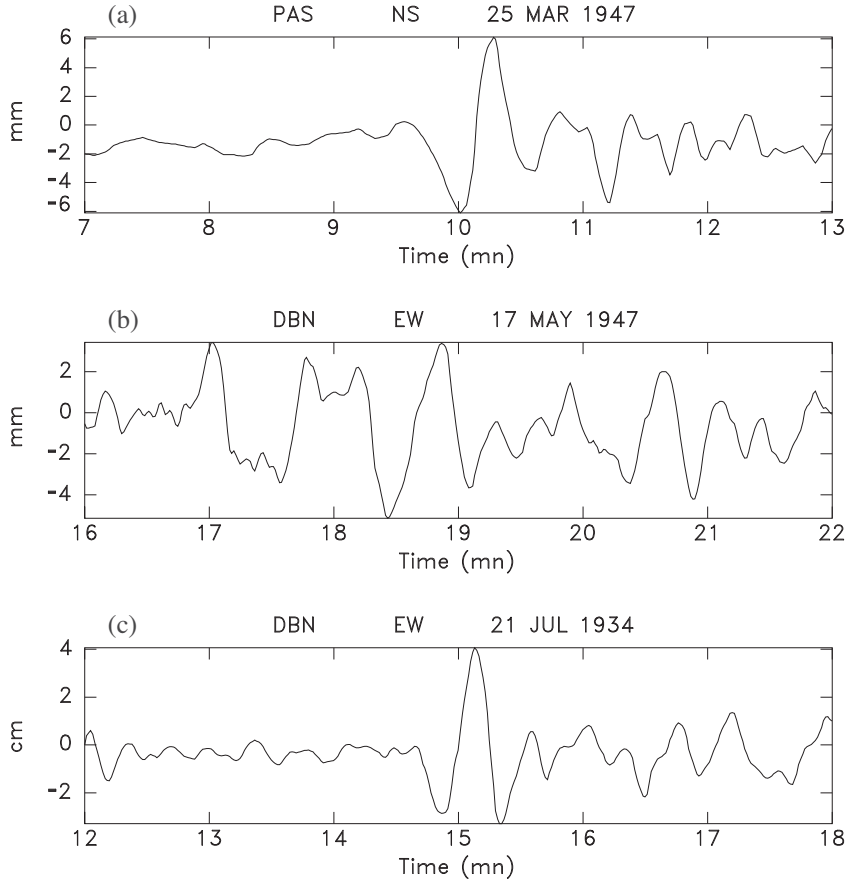

Figure 3. Representative examples of digitized mantle Love waves G_1 used for the evaluation of low-frequency moments: (a) Benioff 70-s strainmeter north–south record at Pasadena for Event I; (b) Golitsyn east–west record at De Bilt for Event II; (c) Golitsyn east–west record at De Bilt for the 1934 Santa Cruz tsunami earthquake.

The mechanisms of the 1947 Hikurangi earthquakes were studied by Doser & Webb (2003), using Downes *et al*. (2001) relocations. They proposed moments of (4–5.1) $\times$ 10^{26} dyn cm for Event I and (2.8–4.5) $\times$ 10^{26} dyn cm for Event II, based on teleseismic body-wave inversions; they were however unable to fully constrain the focal mechanisms. Assuming a low-angle thrust fault at the interface between the Pacific and Australian plates [one of Doser & Webb's (2003) mechanisms], Bell *et al*. (2014) obtained a value of 4.7 $\times$ 10^{26} dyn cm for Event I from the modelling of regional and teleseismic body waves. Most significantly, their results require an exceptionally slow rupture velocity, on the order of 150–300 m s^{-1}, that is, 10–20 times slower than standard rupture velocities and even 3–5 times slower than documented in recent tsunami earthquakes (e.g. Pelayo & Wiens 1992; Kikuchi & Kanamori 1995; López & Okal 2006);[1] the corresponding source duration could be on the order of 300 s.

In this context, we computed the low-frequency source spectra of Events I and II from long-period surface waves. We have shown in a number of previous studies that it is possible to derive the seismic moment of comparably sized events (with moments between 10^{27} and 10^{28} dyn cm) from historical records written on instruments such as the long-period Golitsyn system or the broad-band Benioff 1–90 (e.g. Okal & Borrero 2011; Ebeling *et al*. 2012; Okal 2012). In the present study, we obtained records of mantle waves from Events I and II at Pasadena, Tucson, De Bilt and San Juan, with representative examples of waveforms shown on Fig. 3 (the earthquakes were too small to be meaningfully recorded on Wiechert mechanical instruments). We processed them through the M_m algorithm (Okal & Talandier 1989), with results shown on Fig. 4 in the form of the variation with frequency of the mantle magnitude corrected for focal mechanism and depth, related to seismic moment through:

$$M_c = \log_{10} M_0 - 20, \tag{2}$$

where M_0 is in dyn cm. We use dips of 8° for Event I, as suggested by Bell *et al*. (2014), and of 10° for Event II (Doser & Webb 2003). In the frequency range 6 $-$ 8 mHz, we obtain average values of $\sim$2 and 1 $\times$ 10^{27} dyn cm, respectively for Events I and II, both significantly larger than previously proposed. We also note a significant trend of increase in M_0 with period, reaching values of 4 and 3 $\times$ 10^{27} dyn cm around 5 mHz, respectively for Events I and II. This trend is verified on Fig. 5, which uses a more traditional logarithmic scale for frequency (e.g. López & Okal 2006); it suggests that any source corner frequency would have a very low value, on the order of 3 mHz, which could not be precisely quantified, as it lies beyond our domain of investigation. These results support the conclusions of Bell *et al*. (2014) for Event I and their extension to Event II;

[1] Incidentally, such extremely low rupture velocities would affect the directivity patterns of a far-field tsunami (Ben-Menahem & Rosenman 1972), since they would become comparable to its phase velocity in deep water, and thus rotate the maximum lobe of radiation towards the azimuth of rupture; however, this remark becomes moot in the case of the 1947 earthquakes, which were not large enough to excite an appreciable far-field tsunami in the first place.

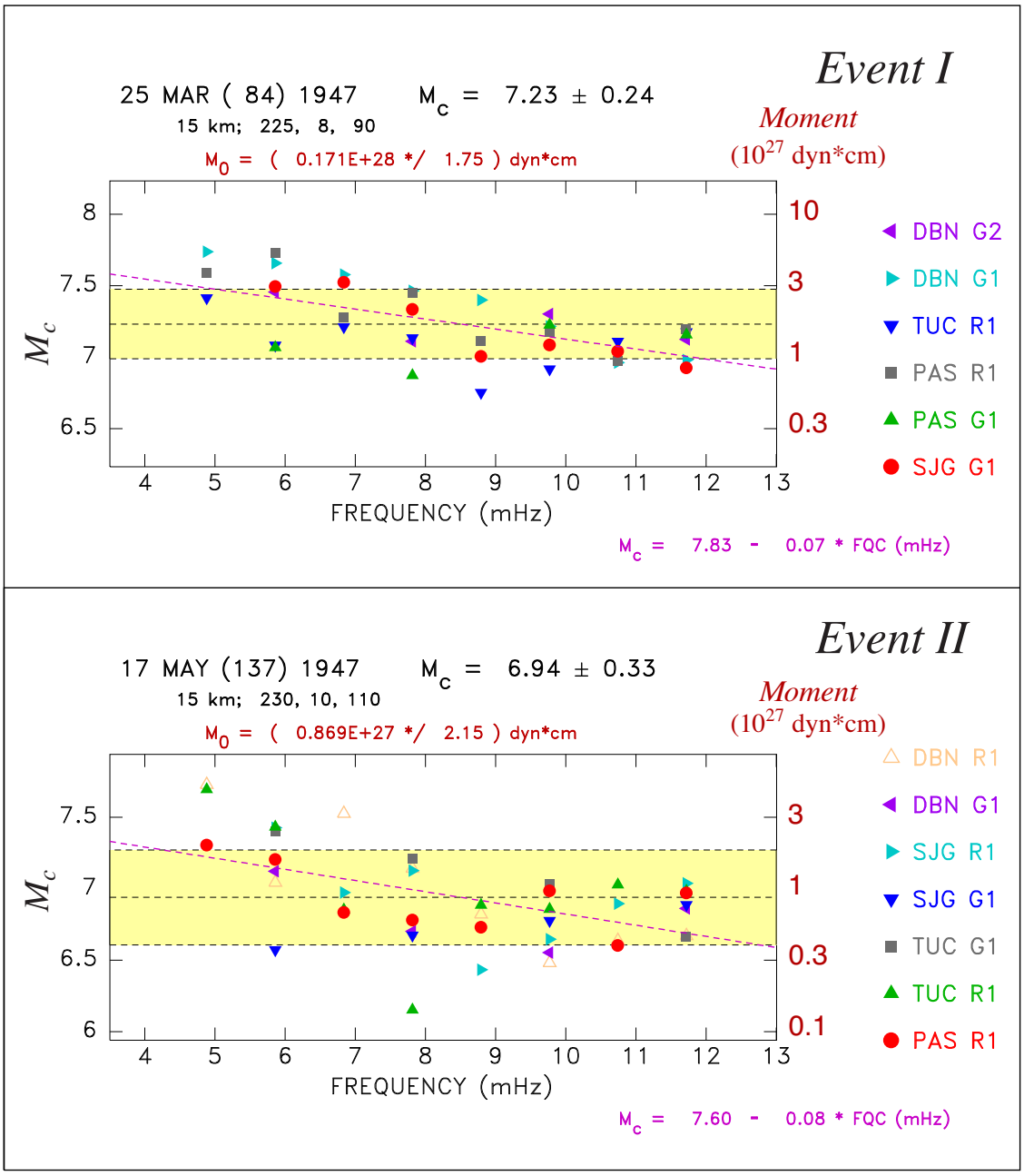

Figure 4. Mantle magnitudes M_c (Okal & Talandier 1989) computed for 1947 Hikurangi Events I (top) and II (bottom). The average value and its 1σ confidence interval are shown as the horizontal dashed line and yellow band. Note the slowness of the events, formalized as the magenta dashed line which regresses the data set with frequency, the slopes (-0.07 and -0.08 logarithmic units per mHz) being characteristic of tsunami earthquakes.

we retain as low-frequency values $M_0 = 4$ and 3×10^{27} dyn cm, respectively for Events I and II, representative of our measurements around 5 mHz.

In this context, we use the slopes of M_c versus frequency f on Fig. 4 as empirical parameters characterizing the slowness of the sources; we have documented in previous studies (Okal & Borrero 2011; Okal 2014) that tsunami earthquakes generally feature slopes on the order of -0.07 logarithmic units per mHz or more (in absolute value) in the 5–12 mHz range (e.g. Java, 2006 (-0.11), and Mentawai, 2010 (-0.08)). By contrast, regular earthquakes feature slopes not exceeding -0.05 (e.g. Maule, 2010 (-0.05), Illapel, 2015 (-0.05), Kaikoura, 2016 (-0.03), the contrast being particularly strong for the 1932 Manzanillo series with slopes of -0.05 (main shock, 3 June), -0.01 (regular main aftershock, 18 June) and -0.14 (tsunami earthquake after-shock, 22 June; Okal & Borrero 2011). In the present case, we obtain values of -0.07 and -0.08 respectively for Events I and II, comparable to those obtained for several tsunami earthquakes.

We note that Doser & Webb (2003) obtained a vastly different mechanism (with a fault strike of 314°, essentially perpendicular to the local plate boundary) when inverting their body-wave data set for Event I using the formalism of McCaffrey & Abers (1988). We have verified that the resulting solution is poorly matched by our mantle wave data set, and thus select the mechanism expressing low-angle subduction, as also preferred by Bell *et al.* (2014).

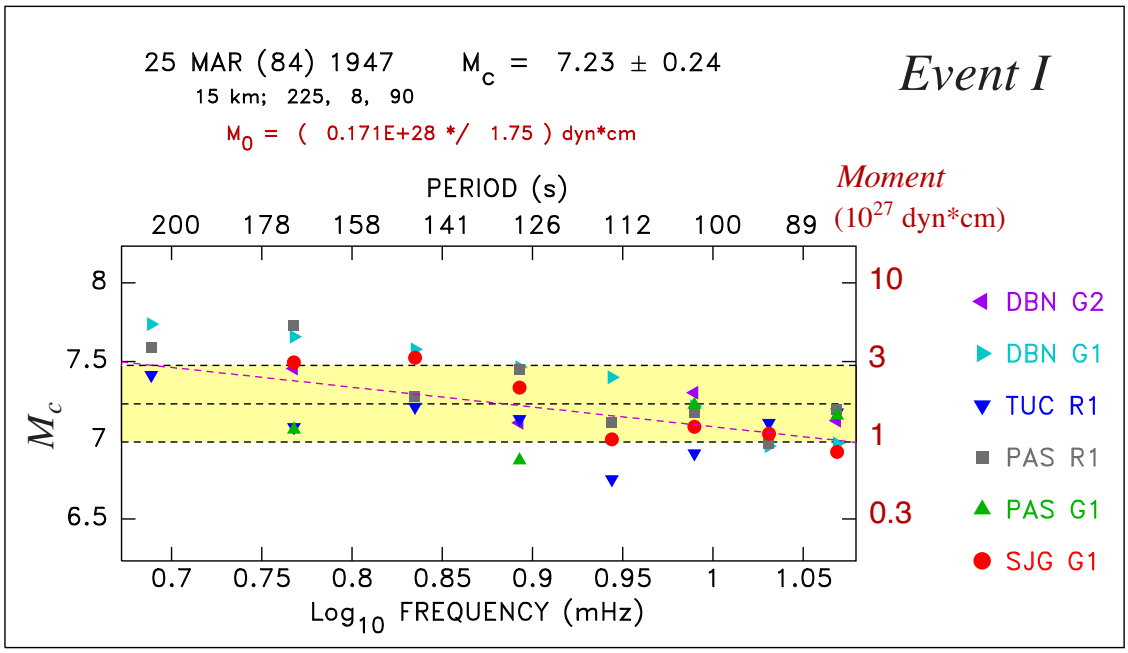

Figure 5. Same as the top frame of Fig. 4, but plotted using a logarithmic scale for frequencies. Note that any corner frequency must be lower than the spectral window used in our study.

In conclusion, our results confirm in the domain of mantle waves the slow nature of both 1947 sources, and their character as tsunami earthquakes, identified at generally shorter periods by the previous authors. They suggest the need for a more quantitative investigation using energy-to-moment ratios and the parameter Θ. Unfortunately, in 1947, there were no stations operating well calibrated short-period instruments in the distance range of Newman & Okal's (1998) algorithm (35°–80°). In addition, the regional records used by Bell *et al*. (2014) were written at distances shorter than allowed in Ebeling & Okal's (2012) extension. By contrast, we were able to obtain records at Tucson (TUC; $\Delta = 96.2°$) for Event I and Pasadena (PAS; $\Delta = 93.0°$) for Event II, which are reproduced on Figs 1(a) and (b), motivating the development of an algorithm to extend the computation of E^E and hence Θ to distances beyond 80°.

3 THE SANTA CRUZ AFTERSHOCK OF 1934 JULY 21 (06:18 GMT)

3.1 Evidence for a tsunami earthquake

This event occurred off Nendö (Santa Cruz) Island, as an aftershock of a major earthquake which took place 3 d earlier off Vanikolo (see Fig. 6). The aftershock on 1934 July 21 is clearly smaller than the main shock on 18 July, with 'Pasadena' magnitudes estimated by Gutenberg & Richter (1954) at $M_{PAS} = 7.3$ and 8.1, respectively. Unfortunately, the only available reports regarding the tsunamis of 18 and 21 July are from the Northern coast of New Caledonia, 1000 km to the South (Anonymous 1935). They describe the arrival of a tsunami in Hienghène and Touho (see Fig. 6) around 8 a.m. local time on the 19th, which fits the expected arrival time from the main shock, assuming the present local time zone (GMT + 11). By contrast, arrivals in Poindimié in the [local] evening on the 19th are difficult to reconcile. The amplitude of the wave was interpreted by Solov'ev & Go (1984b) as a run-up of 0.6 m. Tsunami arrivals from the aftershock are reported at Touho and Thio in the evening of the 21st (they would be expected around 19:00 local time), and described as stronger (if shorter in duration) than for the main shock. In addition, an intriguing harbour oscillation was reported on the 22nd (local time) in Nouméa on the Southern coast of New Caledonia, during an ebbing tide (but with no precise indication of time), while no such phenomenon was described following the main shock. This report is difficult to interpret, since, in order to be observed presumably in daylight, it would require a propagation time of at least 13 hr for a distance (around New Caledonia) not exceeding 1500 km (see Fig. 6); it could involve harbour resonance at a frequency propagating outside the undispersed shallow-water approximation (Okal *et al*. 2006). Nevertheless, these observations generally uphold the character of a tsunami earthquake for the aftershock on 1934 July 21.

This pattern of a seismically smaller event generating a larger tsunami than the main shock constitutes one class of 'tsunami earthquakes', initially described by Fukao (1979) in the Kuril Islands, with other examples including the 1932 Manzanillo series (Okal & Borrero 2011), and the 2010 Mentawai earthquake following the 2007 Bengkulu megathrust event (Borrero *et al*. 2009; Hill *et al*. 2012). They are often modelled as releasing stress transferred by the main shock either onto the shallowest section of the interplate contact or onto splay faults in an accretionary wedge featuring deficient mechanical properties, resulting in decreased rupture velocities and redshifting of the source spectrum towards the lower frequencies responsible for tsunami genesis. Okal (1988) has verified that rupture in softer 'sedimentary' material can amplify tsunami excitation relative to that of seismic waves. We will refer to such events as 'aftershock tsunami earthquakes', or ATEs, as opposed to 'primary tsunami earthquakes' (PTEs) occurring as main shocks (e.g. Aleutian, 1946; Nicaragua, 1992; Java, 1994 and 2006).[2]

[2]Note that we use here the term 'aftershock' in a broad sense, to describe generally smaller earthquakes following in the vicinity of a main event, without the restriction that they should take place on the same fault, a condition that 'true' aftershocks should satisfy, for example if used in the quantification of a rupture area.

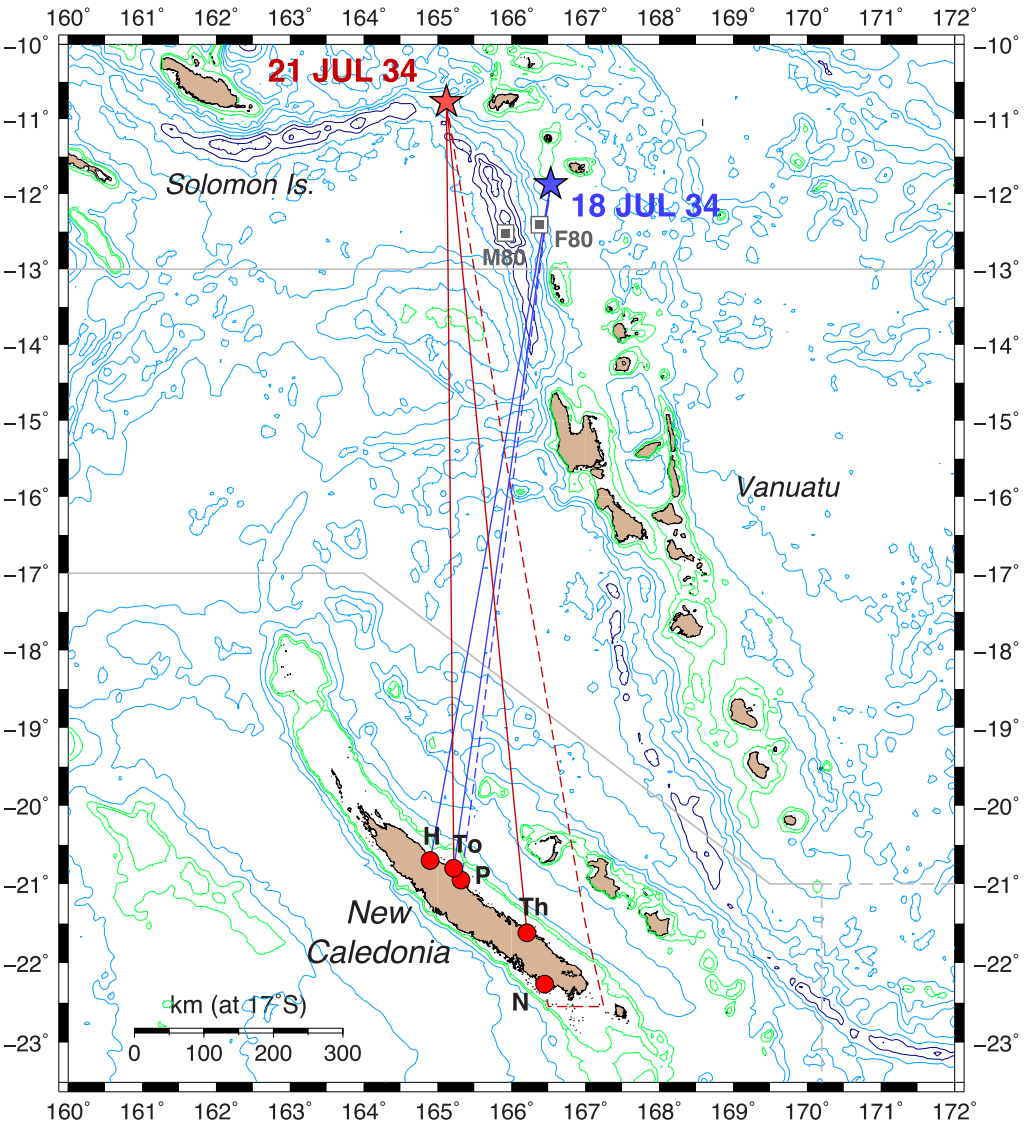

Figure 6. Epicentres of the 1934 Santa Cruz main shock (blue star) and tsunami earthquake (red star), with locations of reported tsunami observations in New Caledonia and probable paths. H: Hienghène; To: Touho; P: Poindimié; Th: Thio; N: Nouméa. See the text for details. The dashed paths refer to the significantly delayed reports at Poindimié and Nouméa. The centred squares are the epicentres of the 1980 foreshock (F80; 8 July) and main shock (M80; 17 July). Isobaths 500 and 1000 m, in green, then at 1000 m intervals; dark blue for depths 6000 m and greater. International boundaries in grey.

In this general context, we conducted a systematic seismological reassessment of the 1934 main-shock–aftershock sequence.

3.2 Relocation of the 1934 Santa Cruz sequence

We relocated the main shock and 16 aftershocks occurring over the next 20 d, using arrival times listed by the International Seismological Summary and the method of Wysession *et al.* (1991), with a larger Gaussian noise standard deviation, $\sigma_G = 5$ s, for an event in the 1930s. Results are listed in Table 1 and mapped on Fig. 7(a). As shown on Fig. 7(d), none of these relocations can resolve depth, but epicentres feature very little moveout when constrained depth varies between 10 and 150 km (small yellow circles on Figs 7b and c), and the local geometry of the Wadati–Benioff zone rules out intermediate or deep foci.

The 1934 main shock locates about 50 km North of the 1980 foreshock–main-shock sequence (F80, M80 on Fig. 6), which featured a classical interplate thrust geometry (e.g. Tajima *et al.* 1990), and also of the large earthquake of 1966 December 31 ($m_b = 5.5$; $M_{PAS} = 7.5$; Fig. 7b). However, as described in Section 5, the latter took place at significant depth (78 km), most probably inside the downgoing slab; its tsunami reached only 2 m on Vanikolo (Solov'ev & Go 1984b).

While our relocations are in general agreement with other published solutions, we note that, in the case of the tsunami earthquake aftershock, both the Centennial catalogue solution (Engdahl & Villaseñor 2002) and the ISC-GEM relocation are significantly offset to the ESE (respectively 60 and 100 km). Incidentally, the quality of all relocations of the 21 July aftershock is systematically poorer than for the main shock: a grade of 'B' as opposed to 'A' for the main shock, assigned by Engdahl & Villaseñor (2002), and a large proportion of arrivals excluded from the data sets (20 out of 85 or 24 per cent in our relocation; 55 out of 202 or 27 per cent for the ISC solution, versus 8 per cent and 3 per cent, respectively for the main shock). This suggests emergent arrivals, as would be expected from a slow earthquake deficient in high frequencies.

Table 1. Relocation of the 1934 Santa Cruz sequence.

Number	Date D M (J) Y	Origin Time GMT	Relocation Latitude (°N)	Relocation Longitude (°E)	Number of arrivals Listed	Number of arrivals Kept	R.M.S. (s)	Magnitude PAS	Remarks
1	**18 JUL (199) 1934**	**19:40:18.9**	**−11.87**	**166.53**	**95**	**87**	**4.45**	**8.1**	**Main shock**
2	18 JUL (199) 1934	21:29:36.2	−12.55	166.08	10	10	5.29		
3	19 JUL (200) 1934	00:06:43.3	−12.57	165.95	48	40	4.77	$6\frac{3}{4}$	
4	19 JUL (200) 1934	05:45:17.5	−13.14	167.27	22	17	5.52	$6\frac{1}{2}$	
5	19 JUL (200) 1934	07:36:56.0	−13.06	165.91	61	50	3.64	6.9	
6	19 JUL (200) 1934	22:57:40.2	−13.09	167.00	10	10	4.65		
7	20 JUL (201) 1934	03:52:25.9	−13.20	166.58	10	10	4.30		
8	20 JUL (201) 1934	16:48:19.6	−12.49	165.70	16	12	3.27		
9	20 JUL (201) 1934	18:05:58.2	−12.77	165.01	6	6	0.59		
10	20 JUL (201) 1934	18:10:23.2	−10.97	165.01	16	14	4.50		
11	20 JUL (201) 1934	18:48:46.8	−10.39	165.34	21	17	4.69		
12	**21 JUL (202) 1934**	**06:18:20.4**	**−10.77**	**165.12**	**85**	**66**	**3.56**	**7.3**	**Tsunami Earthquake**
13	21 JUL (202) 1934	07:22:38.4	−11.06	165.77	21	16	3.54		
14	21 JUL (202) 1934	20:11:27.2	−10.66	166.07	12	10	4.72		
15	22 JUL (203) 1934	02:57:52.8	−10.91	165.38	27	24	4.43	$6\frac{1}{4}$	
16	27 JUL (208) 1934	12:25:38.2	−12.33	166.59	14	13	4.88		
17	07 AUG (219) 1934	03:40:06.4	−12.66	166.65	60	55	2.93	6.9	

Note: All relocations carried at a constrained depth of 10 km.

The relocated aftershocks feature a bimodal distribution, largely correlated with time: during the first 2 d, they cluster around the main shock, suggesting a fault extending Southeast 150 km along the Vanuatu trench. Starting with Event 10 (and perhaps the poorly located Event 9), they move North and cluster around the tsunami earthquake of 21 July (Event 12), suggesting a fault length of 100 km for the latter. The late events, 16 and 17, return to the area of the main shock.

We note further that our relocated epicentre for the tsunami earthquake of 1934 July 21 coincides (within 7 km) with that of the large earthquake of 2013 February 6 ($M_0 = 9.4 \times 10^{27}$ dyn cm; grey centred square symbol on Fig. 7c). That event generated a powerful tsunami running-up 12 m and causing 10 deaths on Nendö Island (Fritz *et al*. 2013), and we have verified that it qualifies as a tsunami earthquake with a parameter $\Theta = -5.94$; it also features a somewhat high ratio of *P*-wave duration to the cubic root of radiated energy E^E, as characterized by their normalized logarithmic ratio Φ (Okal 2013): with $\Phi = 0.38$, the 2013 Santa Cruz event fits marginally above the threshold of 0.35 proposed for slow events including tsunami earthquakes, and is directly comparable to the 2010 Mentawai ATE ($\Phi = 0.39$). The 2013 earthquake has also been recognized as deficient in high frequencies by Lay *et al*. (2013).

3.3 Focal mechanism and moment

Unfortunately, we were unable to build a fully constrained focal mechanism for either the main shock or the aftershock, due to the scarcity and poor azimuthal distribution of stations, and in the case of the tsunami earthquake, to the strongly emergent nature of first arrivals. In the case of the main shock, we have verified that a mechanism slightly adapted from that of the nearby 1980 main shock ($\phi = 338°$; $\delta = 23°$; $\lambda = 93°$) is compatible with the few available first motions, and results in an acceptable scatter of moments for a data set of 13 mantle waves at worldwide stations (Fig. 8), suggesting a low-frequency moment $M_0 = 2.5 \times 10^{28}$ dyn cm. In the case of the tsunami earthquake, we use a mechanism derived from that of the 2013 event, but with a steeper dip ($\phi = 340°$; $\delta = 40°$; $\lambda = 70°$), which yields an average moment of 2.7×10^{27} dyn cm; however, the mantle wave spectra feature a strong growth with period, with an average moment of 7.3×10^{27} dyn cm at 170 s, and a slope of −0.1 logarithmic unit per mHz, suggesting a static moment as large as 10^{28} dyn cm (Fig. 8). Note that these moment values are generally compatible with the faults lengths (150 and 100 km, respectively) suggested by the aftershock distribution (Fig. 7a).

3.4 Record available for the computation of estimated energy

The only record available is the Pasadena short-period vertical (Benioff 1932), whose *P* wave is shown in Fig. 1(c).

4 EXTENSION OF THE Θ ALGORITHM BEYOND 80°

4.1 Methodology

In this section, we define a procedure to obtain a special distance correction in order to compute a value of E^E at distances greater than 80°. For this purpose, we consider a modern reference event for which an ample data set of worldwide digital stations in the range $35° < \Delta < 80°$ allows the routine computation of E^E and hence of a reference value Θ_{ref}, using the standard algorithm of Newman & Okal (1998). We then use digital stations (indexed *i*) recording the same event at distances greater than 80° to study the residual $r_i = \Theta_i - \Theta_{ref}$ as a function of distance, where Θ_i is computed by simply extrapolating the algorithm derived for shorter distances by Newman & Okal (1998). A regressed value of the opposite of the residual can then be used as an empirical correction, allowing an estimate of Θ for the historical event from a single record beyond 80°.

We recall that Newman & Okal's (1998) algorithm corrects the energy flux recorded at a teleseismic station through the combination of geometrical spreading (their eq. 4), and of a squared-average estimate of the radiation coefficient of the generalized *P* wave

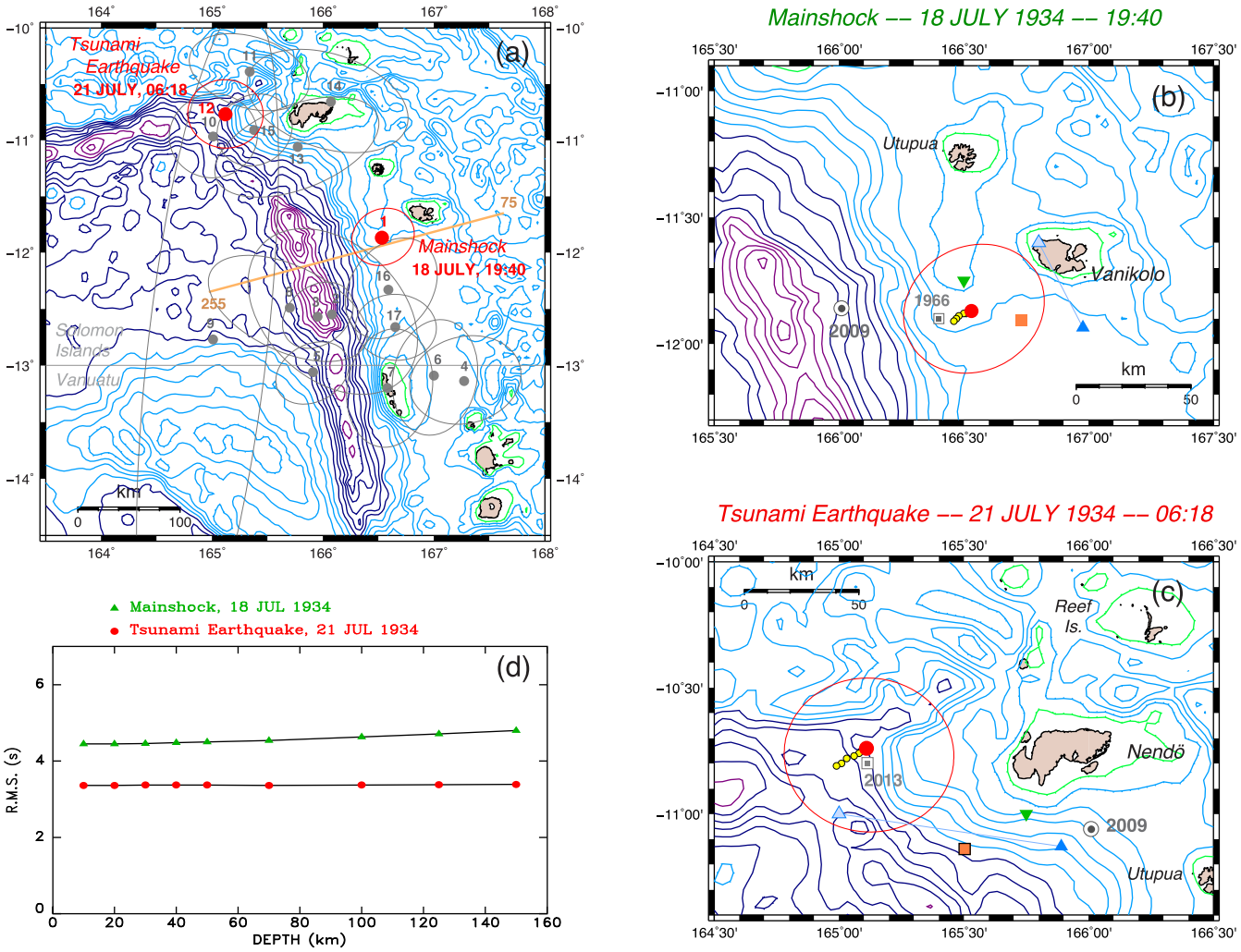

Figure 7. Relocation of the 1934 Santa Cruz sequence. (a) Relocated epicentres shown as solid dots (with numbers keyed to Table 1), with associated Monte Carlo ellipses computed for $\sigma_G = 5$ s. The main shock and tsunami earthquakes are shown in red. Isobaths are at 200 m intervals above 1000 m (green), and deeper at 500 m intervals. The brown line shows the strike of the cross-section on Fig. 15. (b) Close-up of (a) showing the relocation of the main shock. The blue triangles are the original ISS solution (shaded) and the updated ISCGEM one (solid). The green inverted triangle is Gutenberg & Richter's (1954) location. The light brown square is the Centennial epicentre (Engdahl & Villaseñor 2002). The small yellow symbols show the minor moveout of our relocations when the constrained depth is varied from 10 to 150 km. The bull's eye symbol locates the 2009 reference event, and the centred square the deeper 1966 earthquake. (c) Same as (b) for the tsunami earthquake of 1934 July 21. The centred grey square is the epicentre of the slow earthquake of 2013 February 6. (d) Root-Mean-Square residuals for constrained depth relocations as a function of hypocentral depth for the 1934 main shock (green triangles) and tsunami earthquake aftershock (red dots). Note their nearly constant values (especially in the latter case), expressing the lack of resolution of depth by the available travel time data set.

(composed of *P*, *pP* and *sP*), regressed as a function of distance as (Newman & Okal 1998, eq. 9):

$$(F^{\mathrm{Est.}})^2(\Delta) = 1.171 - 7.271 \times 10^{-3}\Delta + 6.009 \times 10^{-5}\Delta^2 \qquad (3)$$

where Δ is in degrees. There are *a priori* two contributions to the residual r_i. One is the inadequacy of the correction (3) beyond the domain of distances for which it was derived; in particular, lateral heterogeneity at the base of the mantle (e.g. Vidale & Hedlin 1998) will result in scattering which will affect both geometrical spreading and the description of attenuation in terms of a parameter t^* taken as independent of distance. The second contribution to r_i is the effect of focal mechanism, which is ignored in the computation of the estimated energy E^E. As discussed in detail by Newman & Okal (1998), in routine computations of the parameter Θ, the use of a large number of stations with a diversity of distances and azimuths provides an adequate sampling and averaging of the focal sphere, allowing the use of the coefficient $(F^{\mathrm{Est.}})^2$ given by (3) to obtain the estimated value of E^E. However, in the case of a single station, the true value of the generalized radiation coefficient may depart significantly from (3), especially if the station lies in the vicinity of a fault plane on the focal sphere.

In the case of the 1947 Hikurangi events, we have verified the absence, in the GlobalCMT catalogue, of any interplate thrust event at latitudes between 40°S and 37°S, with a sufficient moment ($M_0 > 10^{25}$ dyn cm) to be used as a reference event; in this context, we use the Kermadec earthquake of 2003 May 4 (30.53°S; 178.23° W; $M_0 = 1.2 \times 10^{26}$ dyn cm; $M_w = 6.7$). This event features a focal geometry comparable to that of the 1947 events, but being farther North along the trench, it offers a large number of records on the North American continent at distances between 85° and 100°. We compute a standard parameter $\Theta_{\mathrm{ref}} = -4.50$ using 18 stations worldwide, at distances ranging from 35° to 80°. We

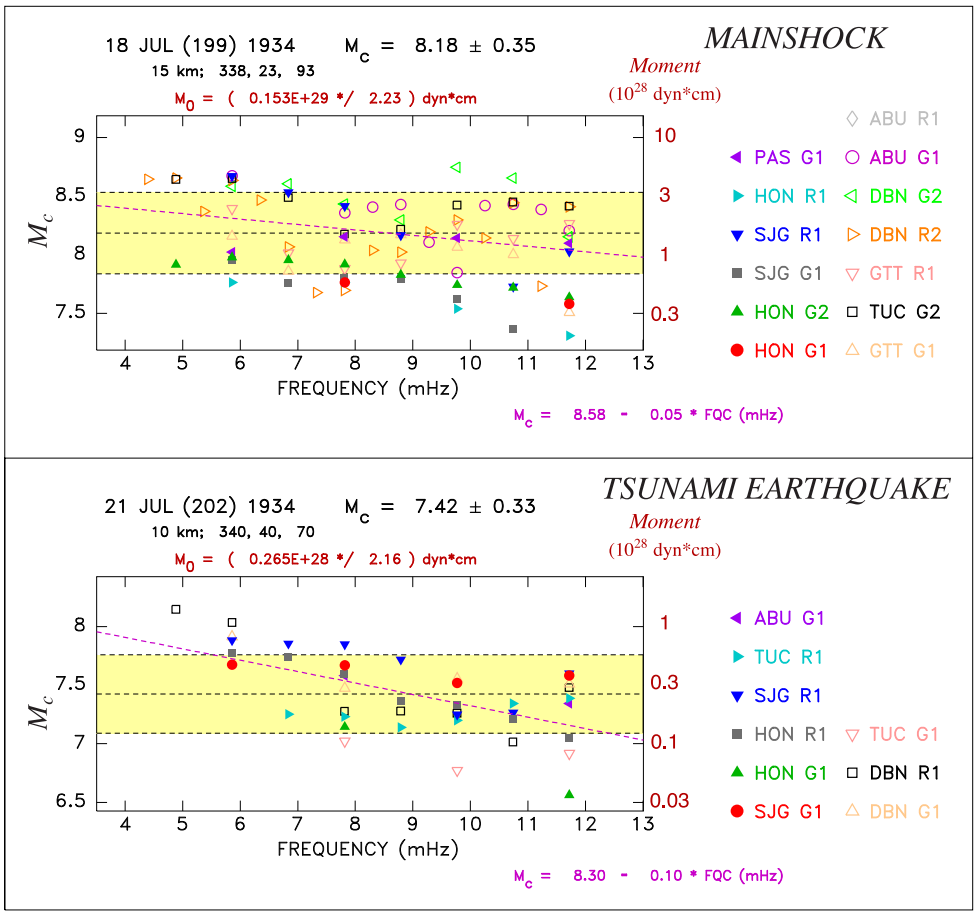

Figure 8. Same as Fig. 4 for the 1934 Santa Cruz main shock (top) and tsunami earthquake aftershock (bottom). Note the strong increase of moment with period for the latter.

then select 37 North American stations at epicentral distances of 86 to 97 degrees, within a $\pm 10^\circ$ window of azimuths at the epicentre (Fig. 9a), and compute values of Θ_i using (3) extrapolated beyond 80° as a distance correction. Results are plotted as residuals r_i on Fig. 10. At distances Δ between 85° and 88.5°, the residual is largely independent of distance, with an average value of -0.37, which we attribute primarily to the effect of focal geometry, expected to result in deficient amplitudes, since the take-off azimuth to North America is close to the fault plane. Starting at about 90°, the residuals become increasingly negative with distance; they can be regressed between 90° and 97° as

$$r = 12.835 - 0.147\Delta = -0.395 - 0.147(\Delta - 90) \qquad (4a)$$

where r is dimensionless (logarithmic units) and Δ is in degrees, as shown by the solid line on Fig. 10.

In the case of the 1934 Santa Cruz tsunami earthquake, we use for reference the event of 2009 October 7 at 11.86°S; 166.01°E ($M_0 = 6.7 \times 10^{27}$ dyn cm; $M_w = 7.8$), which locates in the vicinity of the 1934 main shock (see Fig. 7b). We similarly compute a value $\Theta_{ref} = -5.47$ from 21 records at distances $35^\circ < \Delta < 80^\circ$, and study the residuals r_i at 92 North American stations ranging in distance from 83.5° to 98° (Fig. 11a). The residuals, shown on Fig. 12, can be regressed between 90° and 100° as

$$r = 10.178 - 0.119\Delta = -0.510 - 0.119(\Delta - 90). \qquad (4b)$$

The fact that eqs (4a) and (4b) are different is a reflection of the differences in focal mechanisms between the two events, as well as, probably, in laterally heterogeneous structure of D'' along the two paths. The latter justifies *a posteriori* the conservative upper bound in distances ($\Delta < 80^\circ$) implemented in the routine worldwide algorithm processing modern events for Θ. However, the opposites of the regressed residuals

$$\mathrm{Corr_{NZ}} = 0.395 + 0.147(\Delta - 90) \qquad (5a)$$

and

$$\mathrm{Corr_{SC}} = 0.510 + 0.119(\Delta - 90) \qquad (5b)$$

will remain adequate corrections when implemented to recover Θ from a measurement beyond 90°, respectively in New Zealand and Santa Cruz, as long as the paths sampled in the lower mantle are similar and the focal mechanism and receiver geometries are also comparable. In both instances (Hikurangi 1947 and Santa Cruz 1934), we have selected the reference events specifically to enforce those conditions. In this respect, eqs (5) bears no pretence to be universally applicable.

4.2 Validation of the approach

Before applying the above algorithm to our historical records, we validate it on recent events in the vicinity of the Hikurangi tsunami

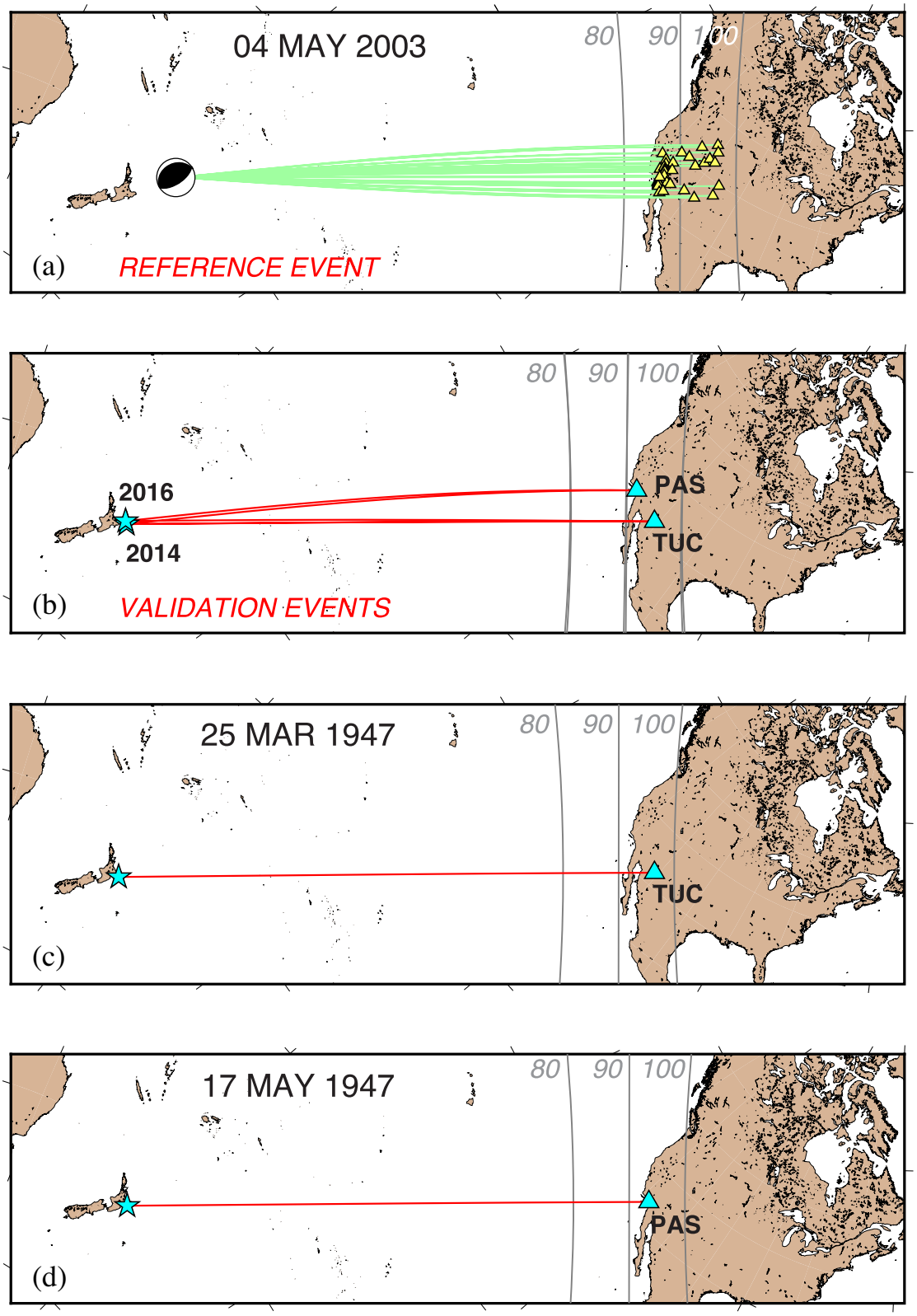

Figure 9. Extension of the Θ algorithm beyond 80° in the geometry of the New Zealand earthquakes. The maps are oblique Mercator projections using the great circle from epicentre to receiver (or centroid to receiver) as the Equator. (a) Reference event of 2003 May 4. The individual stations used to compute the residuals r_i are shown as triangles with the great circle paths as green lines. The grey lines are epicentral isodistals for 80°, 90° and 100°, respectively. (b) Geometry of the validation experiment using the normal faulting events of 2014 and 2016. Note that differences in epicentral location, propagation paths, and isodistals are barely notable on the scale of this map. (c,d) Geometry of the historical paths of 1947.

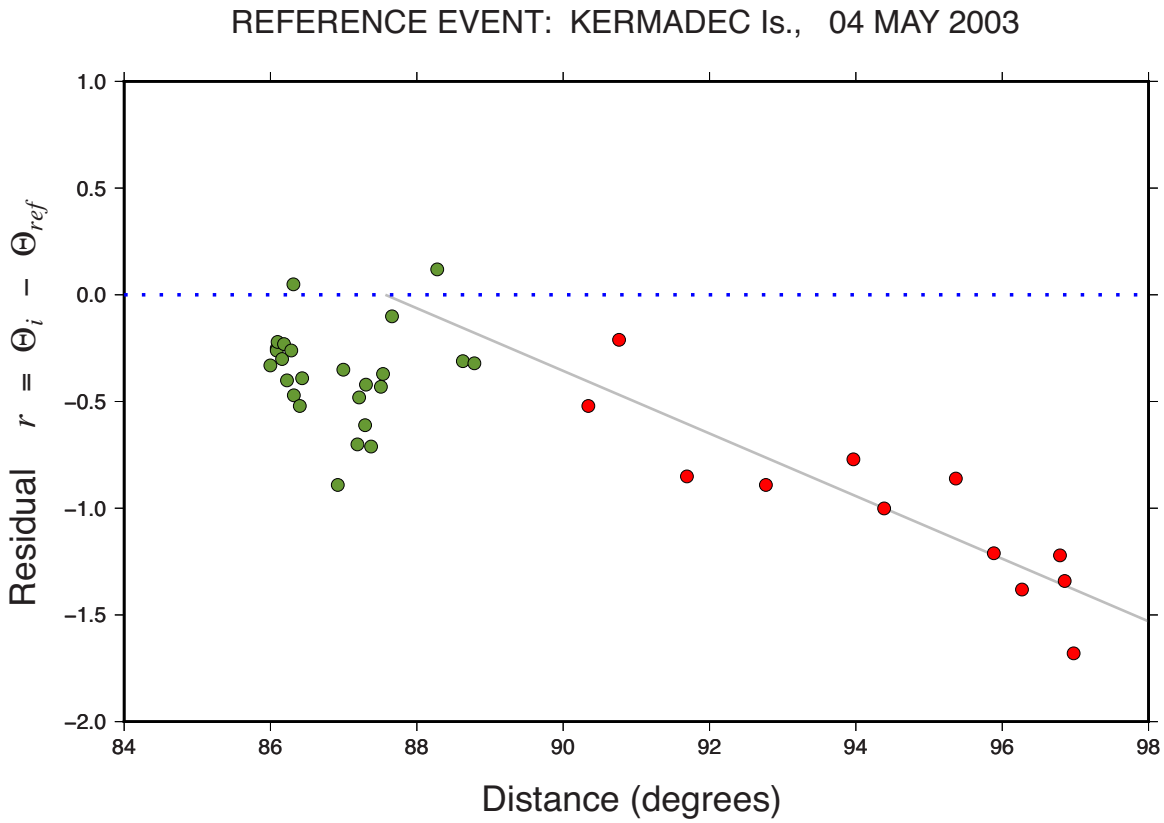

Figure 10. Residuals r_i plotted as a function of distance to North American stations beyond 85° for the reference Kermadec event of 2003 May 4. The solid grey line is the linear regression (5a) of the [red] data points, beyond 89°.

earthquakes. In the absence of interplate thrust events, we consider the two nearby normal faulting earthquakes of 2014 November 16 ($M_0 = 1.3 \times 10^{26}$ dyn cm; $M_w = 6.7$) and 2016 September 1 ($M_0 = 4.2 \times 10^{26}$ dyn cm; $M_w = 7.0$). The validation epicentres are shown on Fig. 2 as bull's eye symbols, and the geometry of the rays to PAS and TUC on Fig. 9(b). While their mechanisms differ from that of the reference earthquake, they share the property that stations in the southwestern US are close to a focal plane, which legitimizes the use of (5a). Using worldwide stations in the 35°–80° distance range, we obtain standard Θ_{ref} parameters of −4.54 (2014) and −4.30 (2016). We then use records at PAS ($\Delta = 91.9°$ and 92.0°, respectively) and TUC ($\Delta = 95.1°$ and 95.2°, respectively) and after using the correction C_{NZ} (5a), obtain Θ values of −4.45 (PAS; 2014), −4.49 (TUC; 2014), −4.12 (PAS; 2016), and −4.21 (TUC; 2016); in all four cases, the residuals with respect to Θ_{ref} are less than 0.2 logarithmic units in absolute value.

This experiment thus validates the algorithm extending the computation of Θ to distances greater than 80° through the use of the corrections (5).

4.3 Application to historical records

All three records shown on Fig. 1 were optically blown-up and digitized at a time sampling of 0.1 s. Instrument responses were obtained from available laboratory ledgers at Caltech for the PAS records (H. Kanamori, personal communication, 2015; see additional discussion in Okal *et al*. 2016); the Appendix details the derivation of the response at TUC in 1947. Computed values of Θ are listed in Table 2.

In the case of Event I (Hikurangi, 1947 March 25) at TUC, we obtained a value of the estimated energy using eq. (3), of $E^E = 2.27 \times 10^{20}$ erg, which with the moment $M_0 = 4 \times 10^{27}$ dyn cm suggested at very long periods from Section 2 and $\mathrm{Corr}_{NZ} = 1.31$ from (5a), yields $\Theta = -5.94$. Similarly, in the case of Event II (Hikurangi, 1947 May 17) at PAS, we obtain $E^E = 1.50 \times 10^{20}$ erg, and with $M_0 = 3 \times 10^{27}$ dyn cm, $\Theta = -6.51$, using $\mathrm{Corr}_{NZ} = 0.89$.

In the case of the Santa Cruz tsunami earthquake of 1934 July 21, we similarly obtain $E^E = 1.41 \times 10^{21}$ erg. However, the distance to PAS is only 85.2°, in a range where (5b) may not apply (green points on Fig. 12). Rather, we use as a correction the opposite of the average residual for that group of points, $\mathrm{Corr}_g = -\overline{r_g} = 0.75$. We have verified that the 2009 residual at PAS (one of the 'green' stations on Fig. 12), $r_{PAS} = -0.78$, is not significantly different from $\overline{r_g}$. With an estimated static moment of 10^{28} dyn cm, this yields a final value of $\Theta = -6.10$ for the event of 1934 July 21, confirming its slow character as a tsunami earthquake. Note that even the more conservative value of the seismic moment $M_0 = 7.2 \times 10^{27}$ dyn cm, which is the average of measured values from mantle waves at 170 s (Fig. 8), still results in a significantly deficient $\Theta = -5.96$.

Results from the three tsunami earthquakes quantified in this study are regrouped on Fig. 13, which provides an update to similar plots by Newman & Okal (1998); Okal (2013), and more recently Okal *et al*. (2016).

In this context, we note that even though some early instruments featured very high magnification (Benioff (1932) experimented with values of up to 100 000 on his short-period seismometer), all of them used analogue recording, which featured a very limited

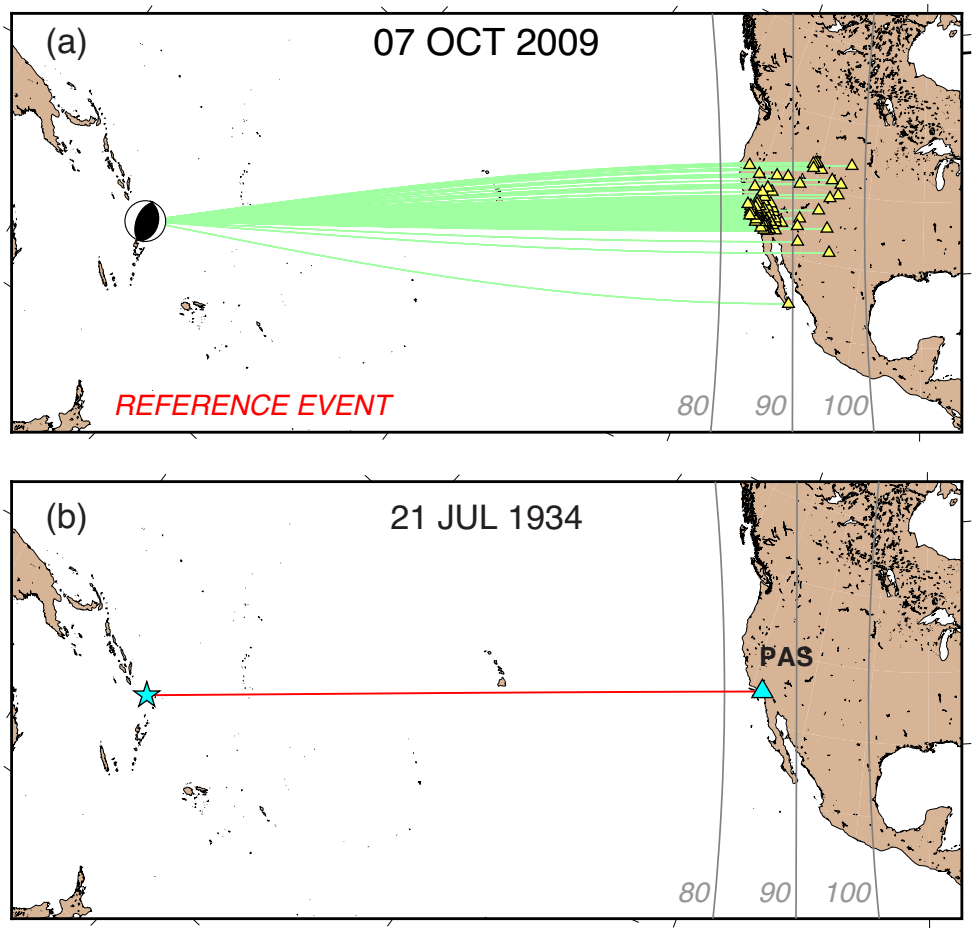

Figure 11. Same as Fig. 9 for the Santa Cruz tsunami earthquake of 1934 July 21. (a) Reference event of 2009 October 7. (b) Application to the historical earthquake.

dynamic range, defined by the ratio of the width of the paper record usable before clipping to that of the ink or light trace, in practice 3, at best 4, orders of magnitude. This is in contrast to the 7 (resp. 9) orders of magnitude achieved by a modern instrument using a 24 (resp. 32)-bit digitizer (e.g. Wielandt 2002). In addition, early short-period instruments had a considerably narrower frequency response than present-day broadband digital ones, which raises the legitimate question of whether they can have an adequate response over the frequency range defining the integral of the energy flux in the frequency domain, typically from 0.1 to 2 Hz. This could conceptually lead to spectral components below noise level at frequencies contributing significantly to radiated energy. However, because of their high maximum magnifications, the short-period instruments used here keep an absolute response comparable to that of the torsion instruments used in the analysis of the 1932 Mexican series (Okal & Borrero 2011), over most of the frequency band relevant to the Parseval integral, and much higher around 1 Hz, where the energy of 'tsunami earthquakes' is typically deficient. Since that study was able to clearly identify a tsunami earthquake of comparable moment (4×10^{27} dyn cm), we expect that our results would not be biased by inadequate frequency response. At any rate, this effect would lead to the processing of background noise into the Fourier integral for energy flux, and thus to an artificial increase in the value of Θ; therefore, it cannot affect our conclusion that the three earthquakes studied are indeed slow.

5 DISCUSSION AND CONCLUSIONS

We have derived an algorithm allowing the use of stations at epicentral distances greater than 80° to compute the slowness parameter Θ introduced by Newman & Okal (1998), a procedure which may be necessary in the study of historical earthquakes having occurred at large distances from the few stations then equipped with short-period instruments.

5.1 Hikurangi Trench

Our application of this method to the 1947 Hikurangi earthquakes allows the quantification of their character as tsunami earthquakes, which was established by the descriptive reports of both felt intensities and tsunami inundation, and the body-wave investigations of Doser & Webb (2003) and Bell *et al*. (2014). By studying the spectrum of mantle waves from both events, we obtain low-frequency moments significantly (but expectedly) larger than derived from body-wave modelling. As shown on Fig. 13, Θ for Event I falls within the range (-6.0 ± 0.1) of the classical PTEs in Java (J94 and J06) and Peru (CP), while Event II ($\Theta = -6.51$) is more comparable to the Nicaragua and El Salvador PTEs (N92 and ES). In this respect, the exceptionally slow ruptures proposed by Bell *et al*. (2014) for Event I need not translate necessarily into extreme values of the parameter Θ. If the source consists of the jagged rupturing of discrete asperities (Polet & Kanamori 2000), radiated energy and hence Θ will be controlled primarily by the rise time of each

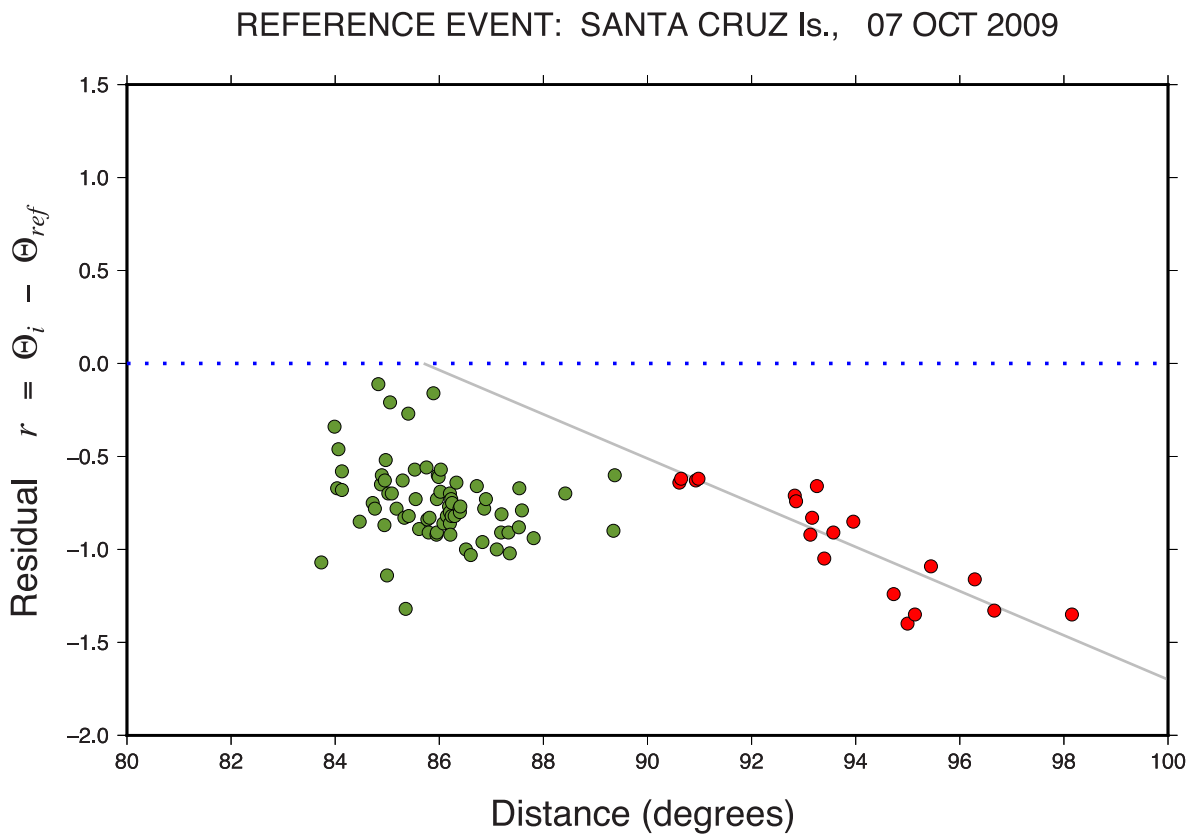

Figure 12. Same as Fig. 10 for the reference event of 2009 October 7 in Santa Cruz. The solid line is the regression (5b).

Table 2. Parameters Θ computed in this study: Hikurangi Trench.

Date D M (J) Y	Origin Time (GMT)	Epicentre (°N)	(°E)	Depth (km)	Moment (10^{27} dyn cm)	Θ	Remarks
04 MAY (124) 2003	13:15:18.7	−30.53	178.23	62	0.12	−4.50	Reference Event (Kermadec Is.)
16 NOV (320) 2014	22:33:20.5	−37.65	179.66	22	0.13	−4.54	Validation Event (Normal faulting)
01 SEP (245) 2016	16:38:14.5	−37.17	179.15	24	0.42	−4.30	Validation Event (Normal faulting)
25 MAR (084) 1947	**20:32:18.8**	**−38.85**	**178.80**	**8**	**4**	**−5.94**	**Tsunami Earthquake**
17 MAY (137) 1947	**07:06:34.7**	**−38.42**	**178.87**	**10**	**3**	**−6.51**	**Tsunami Earthquake**

asperity, and remain relatively insensitive to the time delay between asperities, the latter merely affecting the apparent average rupture velocity.

As mentioned above, these results cannot be compared directly to modern estimates of Θ for nearby events, since the Hikurangi Trench region does not feature even one single entry for a thrust mechanism above 10^{25} dyn cm in the GlobalCMT catalogue. In addition, the 1947 earthquakes are the only ones documented in the historical data set covering the years 1917–1961 analysed by Doser & Webb (2003); between 1962 and 1975, the only thrust faulting event with a reported magnitude $M \geq 6$ is the 1966 Gisborne earthquake for which Webb *et al*. (1985) have computed a moment of only 4×10^{24} dyn cm.

Several fundamental questions regarding the nature of large subduction earthquakes at the Hikurangi Trough thus remain wide open.

(1) First, is the slowness featured in the two 1947 events a regional trend to be expected for all large interplate events in the area? As documented by Okal & Newman (2001) and later confirmed during the 2006 PTE, in the case of the Java Trench, the only known large interplate earthquakes are slow PTEs, with only a few much smaller shocks featuring standard Θ values. By contrast, the same authors identified a wide range of Θ values, albeit for generally smaller events, along the Central American Trench, confirmed by recent seismicity featuring both a PTE (El Salvador, 2012) and a large event with only a trend towards slowness (Costa Rica, 2012; $\Theta = -5.59$). In Northern Peru, Okal & Newman (2001) described slow PTEs on 1996 February 21 (Chimbote) and 1960 November 20, but values only trending towards slowness for the large events of 1966 October 17 and 1974 October 3. In the absence of any other quantifiable interplate thrust event, there can be no answer to this question in the case of the Hikurangi Trench.

(2) In addition, could the Hikurangi Trench sustain a so-called 'mega-thrust' earthquake (with a moment reaching 10^{29} dyn cm)? In the wake of the 2004 Sumatra earthquake (and more recently of the 2011 Tohoku event), the once promising model of Ruff & Kanamori (1980), correlating the simple plate tectonics parameters of plate age and convergence velocity to maximum earthquake size at subduction zones, had to be abandoned (McCaffrey 2007; Stein & Okal 2007). While Schellart & Rawlinson (2013) have indeed listed the Hikurangi Trough as the potential site of a megathrust event, their model, based on an extensive set of plate and morphological properties, remains at this point tentative.

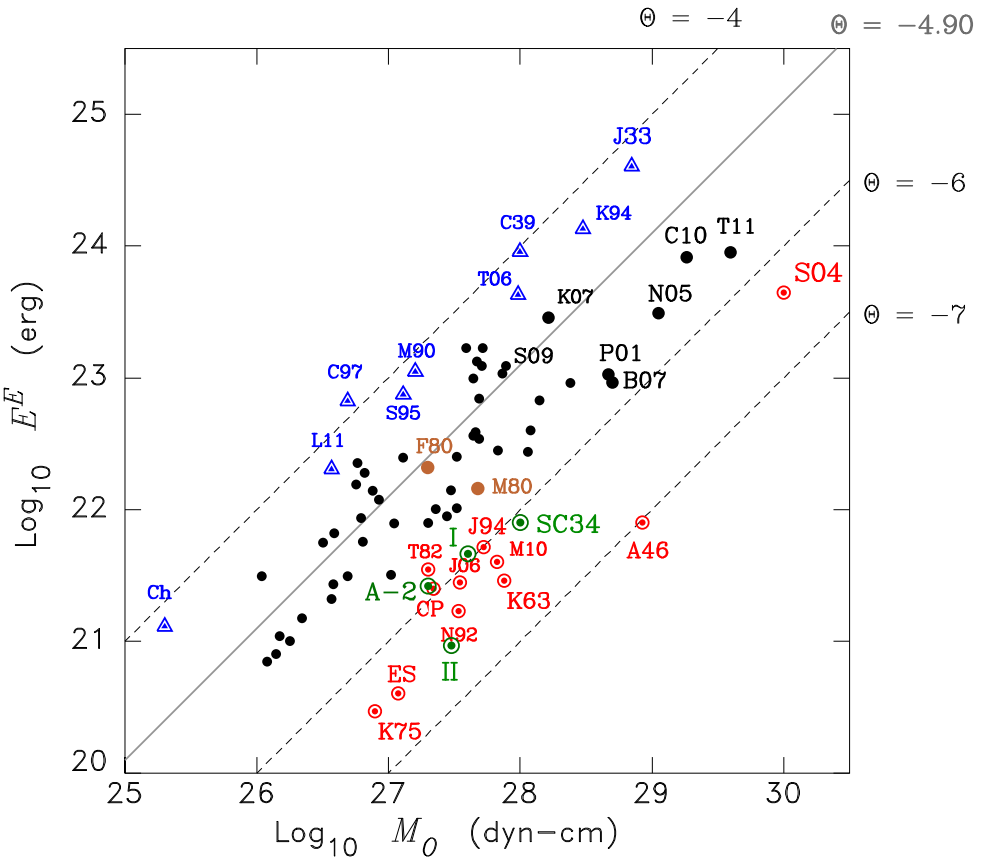

Figure 13. Plot of energy E^E versus moment M_0, updated from the original work of Newman & Okal (1998) and more recently Okal (2013), to include the results of the present study: Hikurangi Events I and II, Santa Cruz ATE (SC34), 1965 ATE (A−2), and 1980 Santa Cruz foreshock (F80) and main shock (M80). Previously studied tsunami earthquakes ($\Theta < -5.8$) are shown as red bull's eye symbols (A46, Aleutian 1946; K63, Kuril 1963 (20 Oct.); K75, Kuril 1975; T82, Tonga 1982; N92, Nicaragua 1992; J94, Java 1994; CP, Chimbote, Peru 1996; S04, Sumatra, 2004; J06, Java 2006; M10, Mentawai 2010; ES, El Salvador, 2012). The blue triangles ($\Theta > -4.3$) identify 'snappy' earthquakes (J33, Sanriku, 1933; C39, Chillán 1939; M90, Marianas 1990; K94, Kuril 1994; S95, Samoa 1995; C97, Chile 1997; T06, Tonga 2006; Ch, Christchurch 2011; L11, Loyalty Is. 2011) and the black dots regular events (P01, Peru 2001; N05, Nias 2005; B07, Bengkulu 2007; K07, Kuril 2007; S09, Samoa 2009; C10, Chile 2010; and T11, Tohoku 2011).

(3) In the affirmative, would such a megathrust event be slow? While the three largest events ever recorded (Chile, 1960; Sumatra, 2004; and Alaska, 1964) all featured source slowness (Kanamori & Cipar 1974; Nettles *et al*. 2005; Stein & Okal 2007), this property was not shared by the 2010 Maule and 2011 Tohoku events (Fig. 13), and the case of the Hikurangi trench remains totally speculative in this respect.

5.2 Santa Cruz and Vanuatu Trench: regional variation of Θ

By contrast, the abundant seismicity of the Santa Cruz−Vanuatu subduction system in the vicinity and to the South of the 1934 ATE earthquake ($\Theta = -6.10$) allows comparison with a number of other events. As mentioned in Section 3.2, we have obtained a very comparable $\Theta = -5.94$ for the 2013 PTE in its immediate vicinity. We have computed systematically slowness parameters for all GlobalCMT solutions in the region since 1990 (to allow for a sufficient development of the global digital network) featuring an interplate thrust mechanism and $M_0 \geq 10^{26}$ dyn cm, as well as for a number of key events before 1990. Results, summarized in Table 3 and mapped on Fig. 14, suggest variations in values of Θ which correlate reasonably well with the local tectonic features of the Santa Cruz−Vanuatu Island chain (Pelletier *et al*. 1998). The right frame on Fig. 14 reproduces the value of Θ as a function of latitude for interplate thrust events, but excludes intraslab (1966), outer rise (1992) and backarc (1999) shocks.

In very general terms, one can distinguish five morphologically different regions:

(1) In the Northern one ('SC' on Fig. 14), the plate interface is poorly coupled, with a well-developed trench reaching 8500 m. Most large interplate thrust earthquakes have $-5.6 \leq \Theta \leq -5.2$ (yellow, with a trend towards slowness), typical of other subduction zones, with only deeper events such as the 1980 foreshock (F80) featuring a standard value around −4.90 (grey). In its Northern part, this segment sustains tsunami earthquakes (red), either as a PTE (2013), or the ATE of a (presumably) regular earthquake (1934).

(2) At the latitude of the Torres Islands ('TI'), the collision of the buoyant West Torres Plateau results in shallowing of the trench to no more than 6000 m and uplifting of the Torres Islands (Taylor *et al*. 1985; Louat & Pelletier 1989). This region is characterized by standard values of Θ, with no known sources featuring slowness or trending towards it; this reflects a stronger level of coupling at the collision zone.

(3) The next segment ('SM') involves the collision of the d'Entrecasteaux system ('d'EFZR' on Fig. 14), a complex feature including both a fossil fracture zone and a passive ridge expressing

Table 3. Parameters Θ computed in this study: Santa Cruz and Vanuatu.

Date D M (J) Y	Origin Time (GMT)	Epicentre (°N)	(°E)	Depth (km)	Moment (10^{27} dyn cm)	Θ	Remarks
07 OCT (280) 2009	22:18:51.2	−11.86	166.01	42	6.7	−5.47	Reference Event
21 JUL (202) 1934	**06:18:20.4**	**−10.77**	**165.12**	**10**	**10**	**−6.10**	**Tsunami Earthquake**
06 FEB (037) 2013	**01:12:25.8**	**−10.80**	**165.11**	**20**	**9.4**	**−5.94**	**Tsunami Earthquake**
1965 Series (Ebel 1980)							
11 AUG (223) 1965	03:40:55.5	−15.47	166.91	23	0.74	−5.26	FS–1
11 AUG (223) 1965	19.52:29.2	−15.64	167.00	20	0.32	−5.45	FS–2
11 AUG (223) 1965	22:31:49.1	−15.75	167.12	28	3.0	−5.55	MS
12 AUG (224) 1965	08:01:44.0	−15.86	167.36	28	0.24	−5.14	A–1
13 AUG (225) 1965	**12:40:08.2**	**−15.88**	**166.83**	**30**	**2.0**	**−5.88**	**A–2; Tsunami Earthquake**
Background Events							
08 JUL (190) 1980	23:19:19.8	−12.92	166.21	44	2.0	−4.92	
17 JUL (190) 1980	19:42:23.2	−12.44	165.94	34	4.8	−5.52	
24 APR (114) 1981	21:50:06.0	−13.51	166.43	44	0.23	−4.89	
15 JUL (196) 1981	07:59:08.5	−17.34	167.27	30	0.58	−5.90	
21 DEC (355) 1985	01:13:21.0	−13.89	166.57	46	0.57	−5.14	
03 JAN (003) 1987	22:04:07.5	−15.06	168.20	17	0.12	−4.90	
28 SEP (271) 1987	11:47:08.6	−18.42	167.79	23	0.19	−5.43	
05 MAR (064) 1990	16:38:15.0	−18.35	168.04	37	0.33	−4.97	
13 FEB (044) 1992	01:29:15.5	−16.14	166.36	15	0.18	−4.54	
12 FEB (043) 1994	17:58:25.0	−20.45	169.04	43	0.33	−4.68	
21 APR (111) 1997	12:02:26.4	−13.21	166.20	51	4.4	−4.91	
26 NOV (330) 1999	13:21:15.5	−16.42	168.21	20	1.67	−4.88	
29 DEC (363) 1999	13:29:19.6	−11.14	165.19	15	0.23	−5.41	
04 OCT (278) 2000	16:58:44.3	−15.51	166.77	15	0.30	−5.01	
02 JAN (002) 2002	17:22:48.8	−17.78	167.85	40	0.77	−4.60	
17 JUN (168) 2002	21:26:22.9	−12.49	166.25	44	0.14	−5.06	
25 MAR (084) 2007	00:40:01.6	−20.60	169.12	41	0.62	−4.52	
25 MAR (084) 2007	01:08:19.0	−20.89	168.99	31	0.27	−4.78	
02 SEP (245) 2007	01:05:18.1	−11.74	165.68	18	0.9	−5.52	
09 APR (100) 2008	12:46:12.7	−20.12	168.80	35	1.1	−5.10	
07 OCT (280) 2009	22:03:14.5	−12.59	166.27	44	3.3	−5.32	
07 OCT (280) 2009	22:50:15.8	−12.59	165.89	18	0.2	−4.01	
07 OCT (280) 2009	23:13:48.2	−13.12	166.37	43.	1.6	−5.05	
08 OCT (281) 2009	08:28:48.0	−13.14	166.09	14	0.16	−5.03	
27 MAY (147) 2010	17:14:46.6	−13.81	166.05	43.	0.69	−4.99	
10 AUG (222) 2010	05:23:45.0	−17.57	167.81	32	1.0	−4.82	
20 AUG (232) 2011	16:55:02.8	−18.52	167.94	34	0.63	−5.34	
20 AUG (232) 2011	18:19:23.5	−18.26	167.94	36	0.46	−4.87	
31 DEC (365) 1966	18:23:09.5	−12.01	166.38	78	4	−5.83	Intraslab, deeper, event

the distortion of bathymetry at the fracture contact (Taylor *et al.* 1980); it has resulted in the complete disappearance of the trench and in the massive uplift of the two largest islands in Vanuatu, Santo and Malekula. This region was the site of the 1965 earthquake swarm, of which the second aftershock (A−2 in Table 3) was recognized by Ebel (1980) as being particularly anomalous; it generated a significant tsunami with 2 m run-up on Santo (Solov'ev & Go 1984b). Despite the large size of the main shock and of A-2, we were able to compute parameters Θ for the five events studied in detail by Ebel (1980), notably by using the correction Corr_{SC} (5b) at high-gain North American stations beyond 90°, where the short-period *P* waves remain on scale; they are plotted as diamonds on Fig. 14. As summarized in Table 3, the Θ values for the 1965 swarm range from standard (A-1) to trending (towards slowness), with A-2 featuring a definitely deficient value (−5.88). We also confirm from mantle waves a relatively high value of the low-frequency moment of A-2 (2×10^{27} dyn cm). Finally, we were able to identify *T* waves from all five major events in the swarm on short-period WWSSN records at Kipapa, Hawaii (but unfortunately not at other island stations in the Pacific). Their small amplitude precludes the quantification of their energy fluxes (Okal 2007), but still allows a qualitative comparison. *T* waves from A-2 are recorded as traces at a level comparable to those of A-1 (despite a moment eight times larger), and significantly weaker than from FS-1 and FS-2, whose moments are 3 and 6 times smaller. They are considerably less intense than the clearly emerging *T* phase from the main shock, whose moment is only ∼1.5 times larger than that of A-2. Such a deficiency in *T*-wave generation is regularly observed in tsunami earthquakes (Okal *et al.* 2003) as a result of a paucity of high frequencies in their source spectrum.

All these properties clearly characterize aftershock A-2 (1965 August 13; 12:40) as an ATE. Note that Centennial catalogue epicentral parameters for the 1965 events (Engdahl & Villaseñor 2003), listed in Table 3 and mapped as the five diamonds on Fig. 14, show that A-2 took place Southwest of the other events in the swarm, and presumably updip from them, in a geometry typical of other ATEs (Fukao 1979; Okal & Borrero 2011).

The only 'snappy' event in this sector, in 1992 ($\Theta = -4.54$), is an outer rise shock which, despite a thrust mechanism, does not represent interplate motion. We exclude it from the right frame of Fig. 14.

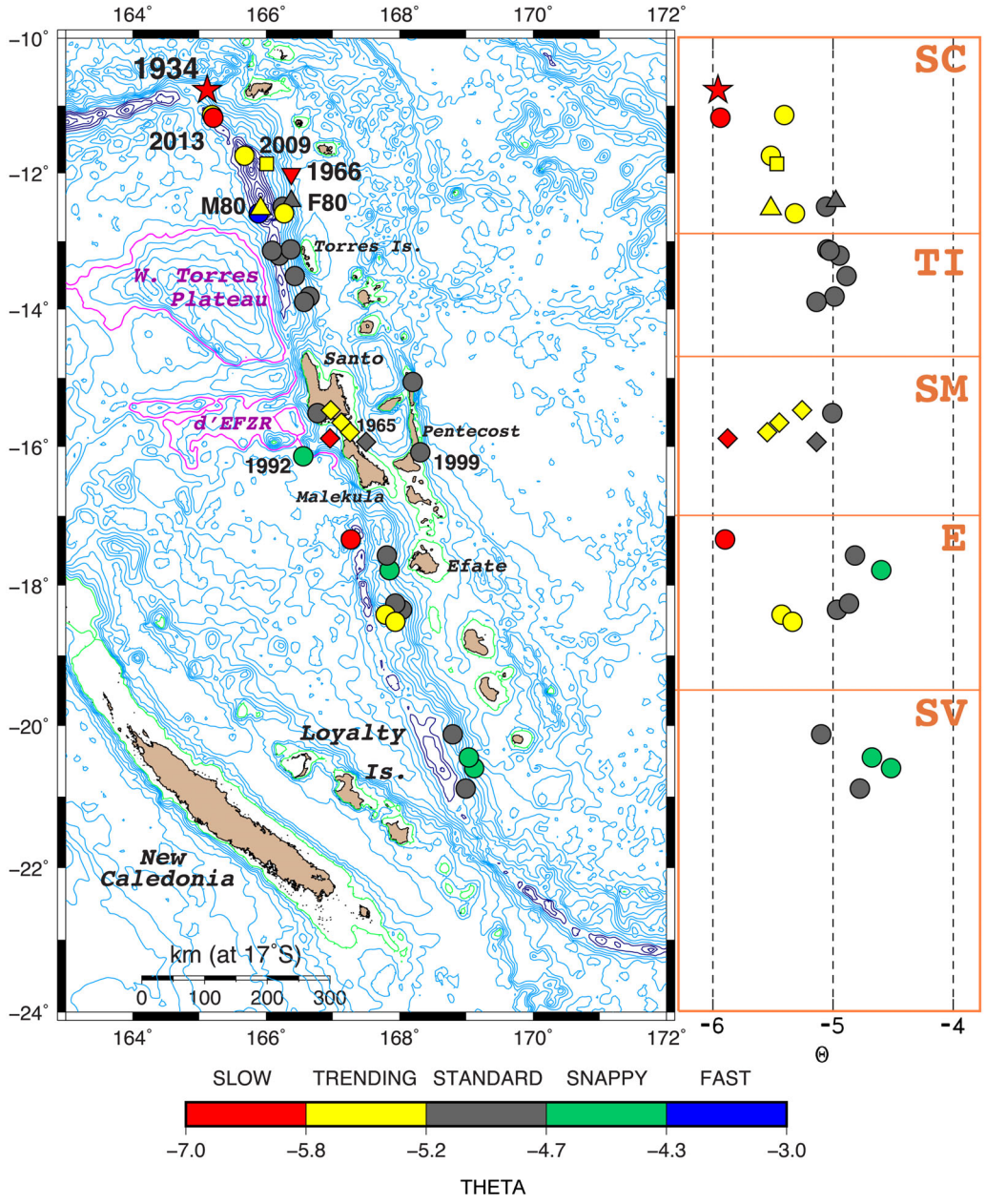

Figure 14. Distribution of parameters Θ for shallow thrust faulting events in Northern Vanuatu and Santa Cruz Islands, colour-coded according to the pallet bar. Left: map view, with the star as the 1934 tsunami earthquake, the square the reference 2009 event, the triangles the 1980 doublet, the diamonds the 1965 swarm, and the inverted triangle the deeper intraslab 1966 event. The West Torres Plateau and the d'Entrecasteaux Fracture Zone and Ridge system are outlined in magenta at the 3500 m isobath. Right: values of Θ plotted as a function of latitude, with the five regional segments outlined in brown. Non-interplate-thrust events have been excluded. See the text for details.

(4) South of the d'EFZR collision, at the latitude of Efate ('E'), the coupling loosens, the morphological expression of the trench reappears, and Θ values return to a more traditional distribution featuring a gradient across the trench, from snappy or standard downdip to trending towards slowness updip. The lone slow event ($\Theta = -5.90$) in 1981 might have qualified as a tsunami earthquake, but for its mediocre size, too small to generate a significant wave in the first place.

(5) Finally in Southern Vanutu ('SV') and despite the presence of a reasonably well defined trench reaching 7000 m, Θ features a standard gradient across the subduction system, but offset towards 'snappier' values. This suggests increased coupling, which may reflect the incipient collision of the Loyalty Islands group.

Our results correlate remarkably well with Wyss *et al.*'s (1983), who mapped on their fig. 10 stress drops inferred from m_b: M_s discrepancies, based on an algorithm by Archambeau (1978). We note in particular the transition from low stress drops in SC to higher ones in TI (labelled ERIR on their fig. 10), back to relatively low values around Efate, and to higher ones in SV. Regarding the SM segment, we note that Wyss *et al.*'s (1983) individual stress drop values (labelled '1' to '4' on their fig. 10) remain significantly lower than in TI (which features several values of '6'), with the exception of both a presumably intraplate event in the general area of our 1992 'snappy' solution, and a number of backarc earthquakes in the vicinity of the 1999 Pentecost event, all of which are not representative of the subduction interface. By contrast, several high

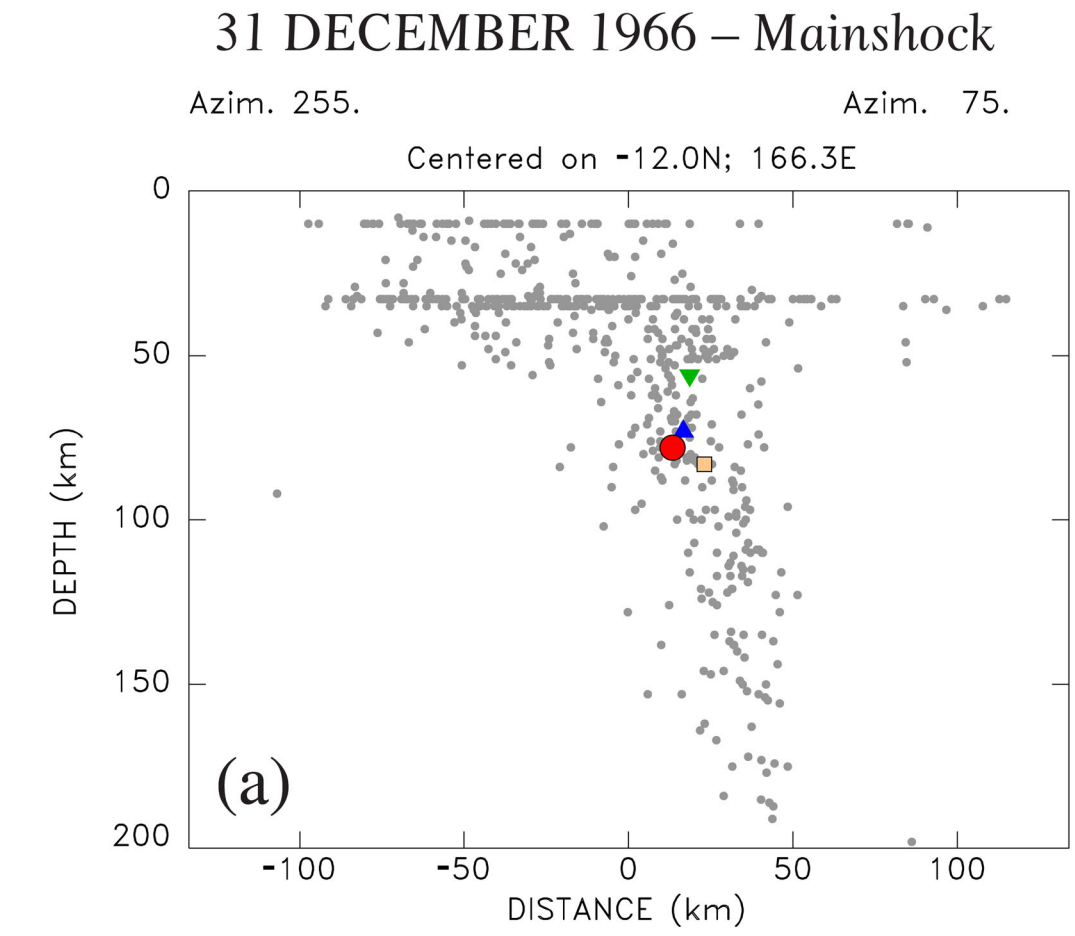

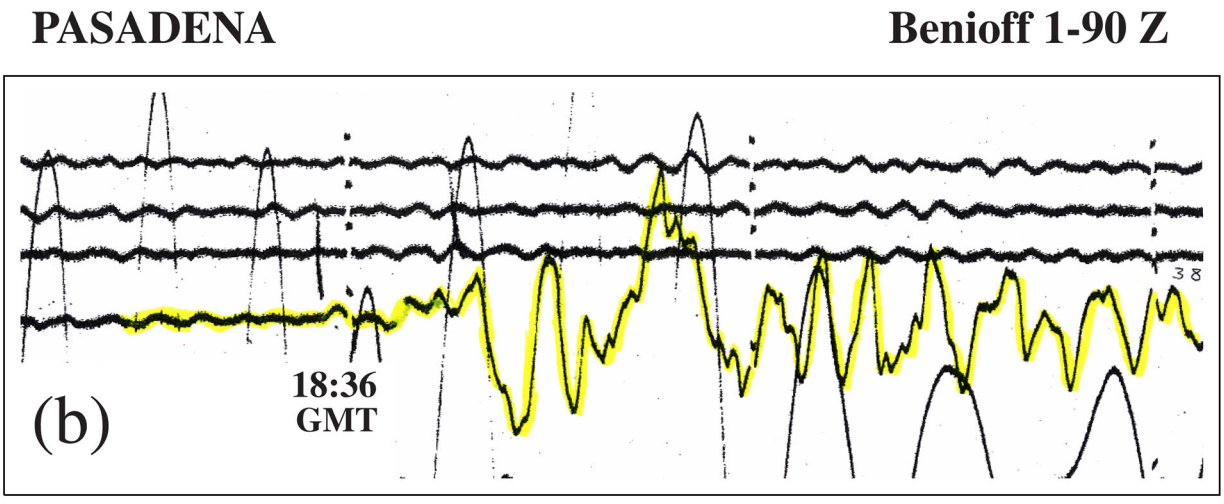

Figure 15. (a) Cross-section of the seismicity of the Vanuatu Wadati–Benioff Zone in the azimuth N75°E (brown line on Fig. 7a). The small grey symbols are unrelocated NEIC hypocentres, the red symbol is our relocation of the large event of 1966 December 31 (18:23 GMT), the blue triangle the ISC location, the green inverted triangle the NEIC one, and the brown square Engdahl & Villaseñor's (2002). (b) Close-up of the *P* wave train recorded on the broad-band vertical 'Benioff 1–90' instrument at Pasadena. The total length of the record is 175 s. Note the virtual absence of high-frequency energy, as compared, for example, with a similar record for the 1939 Chillán, Chile earthquake (Okal & Kirby 2002; Fig. 4).

stress drop shocks (with a label of '6') are present in the 'SV' segment, where we have identified higher values of Θ.

The case of the earthquake of 1966 December 31 (inverted triangle on Fig. 14) is more intriguing. This event, which occurred as the main shock of a complex swarm lasting several days, was given magnitudes $m_b = 5.5$ and $M_{PAS} = 7.5$, suggesting significant source slowness; however, its tsunami was only marginally reported with a maximum run-up of 2 m on Vanikolo (and no known casualties). Johnson & Molnar (1972) published a thrusting focal mechanism ($\phi = 251^\circ$; $\delta = 50^\circ$; $\lambda = 110^\circ$), but with a P axis in the azimuth N327°E, that is, parallel to the trench. Marthelot (1983) later rotated the mechanism to a geometry marginally consistent with first motion data, but in agreement with interplate thrust motion ($\phi = 337^\circ$; $\delta = 47^\circ$; $\lambda = 95^\circ$); on that basis, several authors have interpreted the 1966 event as a genuine interplate thrust earthquake, contributing to the plate motion budget (e.g. Tajima *et al*. 1990; Lay *et al*. 2013). A significant issue with this model is the depth of the source, which was originally given as 56 km by the USGS, and 73 km by the ISC. The modern Centennial catalogue relocation puts it at 83 km (Engdahl & Villaseñor 2002), but the ISC-GEM one uses a constrained depth of 55 km (Storchak *et al*. 2013); our own relocation places it at 78 km, with Monte Carlo hypocentral depths (obtained with $\sigma_G = 1$ s in the 1960s) ranging from 67 to 95 km; as shown on Fig. 15(a), this locates the source inside the subducting slab, rather than at the plate interface; note that this hypocentre is consistent with the mediocre reported tsunami amplitude, and moots the argument against Johnson & Molnar's (1972) mechanism. The analysis of the strong mantle waves at Pasadena yields a moment of 4×10^{27} dyn cm in Johnson & Molnar's (1977) geometry. In general, P waves at most short-period WWSSN stations are off scale, but we were able to process the record at Wellington (WEL), written at a particularly low gain of only 6250, and records in North America at distances greater than 80° [Albuquerque, Golden (WWSSN) and Yellowknife (Canadian Network)], and on the Benioff broadband 1–90 record at PAS, spectacularly devoid of high frequencies (Fig. 15b). With appropriate corrections for the short distance at WEL (Ebeling & Okal 2012) and the large ones ($Corr_g$ or $Corr_{SC}$; see above) in North America, we obtain $\Theta = -5.83 \pm 0.11$, which supports the large difference in m_b and M_{PAS} values and casts the 1966 event as a rather unique example of intraslab earthquake, at the limit between classically defined shallow and intermediate events, featuring a significantly deficient Θ (Saloor & Okal 2015).

6 CONCLUSIONS

We have derived a procedure for the extension to distances $\Delta > 80^\circ$ of the slowness parameter Θ defined by Newman & Okal (1998). This allows the quantification of energy-to-moment ratios when appropriate stations are unavailable in the standard distance range, a situation characteristic of the pre-digital era of seismic recording, when short-period stations were either scarce (as in the case of the 1947 and 1934 events), or analogue instrumentation resulted in off-scale recording of P waves at conventional distances during large earthquakes (a situation typical of the WWSSN during the years 1963–1980).

Because of the influence of lateral heterogeneity in D'' at the high frequencies involved in the computation of estimated energy, we cannot derive a universal correction to the Θ algorithm, but rather must proceed with regionally adapted corrections. Nevertheless, we were able to successfully process three major historical earthquakes. In the Hikurangi province of New Zealand, we confirm the slow character of the two 1947 tsunami earthquakes. Their quantification through the parameter Θ casts Events I and II as comparable to tsunami earthquakes in Java and Northern Peru, and Central America, respectively, with the major difference that no significant background interplate thrust seismicity is known in the region.

In the Santa Cruz Island region, we quantify the event of 1934 July 21 as a tsunami earthquake occurring as an aftershock of a major event, in the immediate vicinity of the recent 2013 primary tsunami earthquake, casting the Santa Cruz corner as a region structurally prone to slow strain release during major events, in either context. Our comprehensive study of source slowness for more recent events along the Santa Cruz−Vanuatu subduction system identifies a wide diversity in parameters Θ, which correlates with variations in tectonic regime in the context of the collision of fossil features born by the subducting Australian plate. Of particular interest is the identification of Aftershock A-2 of the 1965 Santo Island as a tsunami earthquake. This illustrates an additional benefit of the extension of the Θ algorithm beyond 80°, which allows the processing of P-wave data when records at standard distances are systematically off-scale on analogue records constituting the only available database during the WWSSN era. It would be anticipated that many more such records could thus be processed in the future for the quantification of crucially important earthquake sources during that time window (1962–1978). This constitutes one more argument (if need be) for the permanent preservation of the relevant archives, and their eventual transfer to digital support (Okal 2015).

ACKNOWLEDGEMENTS

We thank Bernard Dost, Reinoud Sleeman, James Dewey and Harley Benz for access to the seismological archives at De Bilt and Golden. Hiroo Kanamori provided copies of ancient calibration ledgers of the Caltech seismometers. This research was partly supported by the National Science Foundation, under subcontract from the University of Pittsburgh's Hazards SEES Grant Number OCE-13–31463. Some of the figures were plotted using the GMT software (Wessel & Smith 1991). The paper benefited from the constructive comments of two anonymous reviewers.

REFERENCES

Anderson, J.A. & Wood, H.O., 1925. Description and theory of the torsion seismometer, *Bull. seism. Soc. Am.,* **15,** 1–72.

Anonymous, 1935. Envahissement du littoral par la mer à la Nouvelle-Calédonie au cours de l'année 1934–1935, *Annales de la Commission pour l'Etudes des Raz-de-Marée,* **5,** 37–38.

Archambeau, C.B., 1978. Estimation of non-hydrostatic stress in the Earth by seismic methods: Lithospheric stress levels along Pacific and Nazca plate subduction systems. Open-File Rep., *U.S. Geol. Surv.,* 78–943, 47–138.

Bell, R., Holden, C., Power, W., Wang, X. & Downes, G., 2014. Hikurangi margin tsunami earthquake generated by slow seismic rupture over a subducted seamount, *Earth planet. Sci. Lett.,* **397,** 1–9.

Ben-Menahem, A. & Rosenman, M., 1972. Amplitude patterns of tsunami waves from submarine earthquakes, *J. geophys. Res.,* **77,** 3097–3128.

Benioff, V.H., 1932. A new vertical seismograph, *Bull. seism. Soc. Am.,* **22,** 155–169.

Bilek, S.L. & Lay, T., 2002. Tsunami earthquakes possibly widespread manifestations of frictional conditional stability, *Geophys. Res. Lett.,* **29,** 1673, 4 pp.

Boatwright, J. & Choy, G.L., 1986. Teleseismic estimates of the energy radiated by shallow earthquakes, *J. geophys. Res.,* **91,** 2095–2112.

Borrero, J.C., Weiss, R., Okal, E.A., Hidayat, R., Suranto, Arcas, D. & Titov, V.V., 2009. The tsunami of 12 September 2007, Bengkulu Province, Sumatra, Indonesia: post-tsunami survey and numerical modeling, *Geophys. J. Int.,* **178,** 180–194.

Charlier, C. & van Gils, J.-M., 1953. *Catalogue des stations séismologiques mondiales,* Observatoire Royal de Belgique, Uccle.

Doser, D.I. & Webb, T.H., 2003. Source parameters of large historical (1917–1961) earthquakes, North Island, New Zealand, *Geophys. J. Int.,* **152,** 795–832.

Downes, G.L., Webb, T., McSaveny, M., Darby, D., Doser, D., Chaguè-Goff, C. & Barnett, A., 2001. The 26 March and 17 May 1947 Gisborne earthquakes and tsunami: implications for tsunami hazard for the east coast, North Island, New Zealand, in: *Tsunami Risk Assessment Beyond 2000: Theory, Practice and Plans,* Proc. Intl. Tsunami Workshop, pp. 14–16, Moscow.

Ebel, J.E., 1980. Source processes of the 1965 New Hebrides Islands earthquakes inferred from teleseismic waveforms, *Geophys. J. R. astr. Soc.,* **63,** 381–403.

Ebeling, C.W. & Okal, E.A., 2012. An extension of the E/M_0 tsunami earthquake discriminant Θ to regional distances, *Geophys. J. Int.,* **190,** 1640–1656.

Ebeling, C.W., Okal, E.A., Kalligeris, N. & Synolakis, C.E., 2012. Modern seismological reassessment and tsunami simulation of historical Hellenic Arc earthquakes, *Tectonophysics,* **530,** 225–239.

Eiby, G.A., 1947. Two New Zealand tsunamis, *J. Roy. Soc. N.Z.,* **12,** 337–351.

Engdahl, E.R. & Villaseñor, A., 2002. Global seismicity: 1900–1999, in *International Earthquake and Engineering Seismology, Part A,* pp. 665–690, eds Lee, W.H.K., Kanamori, H., Jennings, P.C. & Kisslinger, C., Elsevier.

Fritz, H.M., Papantoniou, A., Biukoto, L. & Gilly, A., 2013. The Solomon Islands tsunami of 6 February 2013 field survey in the Santa Cruz Islands, *EOS, Trans. Am. geophys. Un.,* **95**(53), NH41A–1696 [abstract].

Fukao, Y., 1979. Tsunami earthquakes and subduction processes near deep-sea trenches, *J. geophys. Res.,* **84,** 2303–2314.

Garnero, E.J. & Helmberger, D.V., 1996. Seismic detection of a thin laterally varying boundary layer at the base of the mantle beneath the Central Pacific, *Geophys. Res. Lett.,* **23,** 977–980.

Glover, D.P. & Meyers, H., 1987. Historical seismogram filming project: Current status, in *Historical Seismograms and Earthquakes of the World,* pp. 373–379, eds Lee, W.H.K., Meyers, H. & Shimazaki, K., Academic Press.

Goodstein, J.R., Kanamori, H. & Lee, W.H.K., 1980. Seismology microfiche publications from the Caltech archives, *Bull. seism. Soc. Am.,* **70,** 657–658.

Gutenberg, B. & Richter, C.F., 1954. *Seismicity of the Earth and Associated Phenomena,* 310 pp., Princeton Univ. Press.

Hill, E.M. *et al.*, 2012. The 2010 $M_w = 7.8$ Mentawai earthquake: very shallow source of a rare tsunami earthquake determined from tsunami field survey and near-field GPS data, *J. geophys. Res.,* **117,** B06402, doi:10.1029/2012JB009159.

Johnson, T. & Molnar, P., 1972. Focal mechanisms and plate tectonics of the Southwest Pacific, *J. geophys. Res.,* **77,** 5000–5032.

Kanamori, H., 1972. Mechanism of tsunami earthquakes, *Phys. Earth planet. Inter.,* **6,** 346–359.

Kanamori, H. & Cipar, J.J., 1974. Focal process of the great Chilean earthquake, May 22, 1960, *Phys. Earth planet. Inter.,* **9,** 128–136.

Kikuchi, M. & Kanamori, H., 1995. Source characteristics of the 1992 Nicaragua tsunami earthquake inferred from teleseismic body waves, *Pure appl. Geophys.,* **144,** 441–453.

Lay, T., Ye, L., Kanamori, H., Yamazaki, Y., Cheung, K.F. & Ammon, C.J., 2013. The February 6, 2013, $M_w = 8.0$ Santa Cruz Islands earthquake and tsunami, *Tectonophysics,* **608,** 1109–1121.

López, A.M. & Okal, E.A., 2006. A seismological reassessment of the source of the 1946 Aleutian "tsunami" earthquake, *Geophys. J. Int.,* **165,** 835–849.

Louat, R. & Pelletier, B., 1989. Seismotectonics and present-day relative plate motions in the New Hebrides – North Fiji Basin region, *Tectonophysics,* **167,** 41–55.

Marthelot, J.-M., 1983. Patterns of seismicity in the Vanuatu (New Hebrides) arc: regional variations and systematic evolution, *PhD Dissertation*, Cornell Univ., Ithaca, 127 pp.

McCaffrey, R., 2007. The next great earthquake, *Science,* **315,** 1675–1676.

Nettles, M., Ekström, G., Dziewoński, A.M. & Maternovskaya, N., 2005. Source characteristics of the great Sumatra earthquake and its aftershocks, *EOS, Trans. Am. geophys. Un.,* **86** (18), JA11 [abstract].

Newman, A.V. & Okal, E.A., 1998. Teleseismic estimates of radiated seismic energy: the E/M_0 discriminant for tsunami earthquakes, *J. geophys. Res.,* **103,** 26 885–26 898.

Okal, E.A., 1988. Seismic parameters controlling far-field tsunami amplitudes: a review, *Nat. Hazards,* **1,** 67–96.

Okal, E.A., 2007. The generation of *T* waves by earthquakes, *Adv. Geophys.,* **49,** 1–65.

Okal, E.A., 2008. The excitation of tsunamis by earthquakes, in *The Sea: Ideas and Observations on Progress in the Study of the Seas,* **vol. 15,** pp. 137–177, eds Bernard, E.N. & Robinson, A.R., Harvard Univ. Press.

Okal, E.A., 2012. The South of Java earthquake of 11 September 1921: a negative search for a large interplate thrust event at the Java Trench, *Geophys. J. Int.,* **190,** 1657–1672.

Okal, E.A., 2013. From 3-Hz *P* waves to ${}_0S_2$: No evidence of a slow component to the source of the 2011 Tohoku earthquake, *Pure appl. Geophys.,* **170,** 963–973.

Okal, E.A., 2014. Far-field tsunami detection and warning, 1854–2014: one hundred and sixty years in the intricate relation between earthquake source and tsunami, *Seismol. Res. Letts.,* **85,** 522 [abstract].

Okal, E.A., 2015. Historical seismograms: preserving an endangered species, *Geo. Res. J.,* **6,** 53–64.

Okal, E.A. & Borrero, J.C., 2011. The "tsunami earthquake" of 1932 June 22 in Manzanillo, Mexico: seismological study and tsunami simulations, *Geophys. J. Int.,* **187,** 1443–1459.

Okal, E.A. & Kirby, S.H., 2002. Energy-to-moment ratios for damaging intraslab earthquakes: preliminary results on a few case studies, *Open File Rep*., *U.S. Geol. Surv.,* 02–328, 127–131.

Okal, E.A. & Newman, A.V., 2001. Tsunami earthquakes: the quest for a regional signal, *Phys. Earth planet. Inter.,* **124,** 45–70.

Okal, E.A. & Talandier, J., 1989. M_m: a variable period mantle magnitude, *J. geophys. Res.,* **94,** 4169–4193.

Okal, E.A., Alasset, P.-J., Hyvernaud, O. & Schindelé, F., 2003. The deficient *T* waves of tsunami earthquakes, *Geophys. J. Int.,* **152,** 416–432.

Okal, E.A., Fritz, H.M., Raveloson, R., Joelson, G., Pančošková, P. & Rambolamanana, G., 2006. Madagascar field survey after the December 2004 Indian Ocean tsunami, *Earthq. Spectra,* **22,** S263–S283.

Okal, E.A., Kirby, S.H. & Kalligeris, N., 2016. The Showa Sanriku earthquake of 1933 March 2: a global seismological reassessment, *Geophys. J. Int.,* **206,** 1492–1514.

Pelayo, A.M. & Wiens, D.A., 1992. Tsunami earthquakes: Slow thrust-faulting events in the accretionary wedge, *J. geophys. Res.,* **97,** 15 321–15 337.

Pelletier, B., Calmant, S. & Pillet, R., 1998. Current tectonics of the Tonga–New Hebrides region, *Earth planet. Sci. Lett.,* **164,** 263–276.

Polet, J. & Kanamori, H., 2000. Shallow subduction zone earthquakes and their tsunamigenic potential, *Geophys. J. Int.,* **142,** 684–702.

Ruff, L.J. & Kanamori, H., 1980. Seismicity and the subduction process, *Phys. Earth planet. Inter.,* **23,** 240–252.

Saloor, N. & Okal, E.A., 2015. Energy-to-moment ratios for deep earthquakes: no evidence for scofflaws, *EOS, Trans. Am. geophys. Un.,* **96** (53), T21D–2851 [abstract].

Schellart, W.P. & Rawlinson, N., 2013. Global correlations between maximum magnitudes of subduction zone interface thrust earthquakes and physical parameters of subduction zones, *Phys. Earth planet. Inter.,* **225,** 41–67.

Solov'ev, S.L. & Go, C., 1984a. Catalogue of tsunamis on the Eastern shore of the Pacific Ocean, *Can. Transl. Fish. Aquat. Sci.,* **5078,** 293 pp.

Solov'ev, S.L. & Go, C., 1984b. Catalogue of tsunamis on the Western shore of the Pacific Ocean, *Can. Transl. Fish. Aquat. Sci.,* **5077,** 439 pp.

Stein, S. & Okal, E.A., 2007. Ultra-long period seismic study of the December 2004 Indian Ocean earthquake and implications for regional tectonics and the subduction process, *Bull. seism. Soc. Am.,* **97,** S279–S295.

Storchak, D.A., Di Giacomo, D., Bondár, I., Engdahl, E.R., Harris, J., Lee, W.H.K., Villaseñor, A. & Bormann, P., 2013. Public release of the ISC-GEM global instrumental earthquake catalogue (1900–2009), *Seismol. Res. Lett.,* **84,** 810–815.

Tajima, F., Ruff, L.J., Kanamori, H., Zhang, J. & Mogi, K., 1990. Earthquake source processes and subduction regime in the Santa Cruz Islands region, *Phys. Earth planet. Inter.,* **61,** 269–290.

Tanioka, Y., Ruff, L.J. & Satake, K., 1997. What controls the lateral variation of large earthquake occurrence along the Japan trench?, *Island Arc,* **6,** 261–266.

Taylor, F.W., Isacks, B.L., Jouannic, C., Bloom, A.L. & Dubois, J., 1980. Coseismic and Quaternary vertical tectonic movements, Santo and Malekula Islands, New Hebrides island arc, *J. geophys. Res.,* **85,** 5367–5381.

Taylor, F.W., Jouannic, C. & Bloom, A.L., 1985. Quaternary uplift of the Torres Islands, Northern New Hebrides frontal arc: comparison with Santo and Malekula Islands, Central New Hebrides frontal arc, *J. Geol.,* **93,** 419–438.

Vidale, J.E. & Hedlin, M.A.H., 1998. Evidence for partial melt at the core-mantle boundary north of Tonga from the strong scattering of seismic waves, *Nature,* **391,** 682–685.

Webb, T.H., Wesnousky, S.G. & Helmberger, D.V., 1985. A body-wave analysis of the 1966 Gisborne, New Zealand, earthquake, *Tectonophysics,* **113,** 271–282.

Weinstein, S.A. & Okal, E.A., 2005. The mantle wave magnitude M_m and the slowness parameter Θ: five years of real-time use in the context of tsunami warning, *Bull. seism. Soc. Am.,* **95,** 779–799.

Wessel, P. & Smith, W.H.F., 1991. Free software helps map and display data, *EOS, Trans. Am. geophys. Un.,* **72,** 441 and 445–446.

Wielandt, E., 2002. Seismometry, in *International Hanbook of Earthquake and Engineering Seismology, Part A,* pp. 283–304, eds Lee, W.H.K., Kanamori, H., Jennings, P.C. & Kisslinger, C., Academic Press.

Wysession, M.E., Okal, E.A. & Miller, K.L., 1991. Intraplate seismicity of the Pacific Basin, 1913–1988, *Pure appl. Geophys.,* **135,** 261–359.

Wyss, M., Habermann, R.E. & Heiniger, C., 1983. Seismic quiescence, stress drops, and asperities in the New Hebrides arc, *Bull. seism. Soc. Am.,* **73,** 219–236.

APPENDIX: DETERMINATION OF 1947 SHORT-PERIOD INSTRUMENT MAGNIFICATION AT TUCSON (TUC)

The short-period record at Tucson used for the Hikurangi earthquake of 1947 March 25 was written on a Benioff short-period seismometer (Benioff 1932). Its mechanical properties (pendulum period $T_p = 1$ s; galvanometer period $T_g = 0.24$ s) are described on the film rolls of the Historical Seismogram Filming Project (HSFP; Glover & Meyers 1987), and reported in Charlier and van Gils' (1953) generally authoritative catalogue. However, the most critical parameter, namely the maximum magnification, V_{max}, is not documented on the rolls; a value of 3×10^4 is listed by Charlier & van Gils (1953) for the broadband combination ($T_p = 1$ s; $T_g = 77$ s) reproducing (with a slightly shorter galvanometer period) the famous Pasadena '1–90' instrument (Fig. A1a), but this is excessive since typical magnifications used for this type of instrument were in the range of 3000, that is, a factor of 10 smaller. We surmise that the listed value of 3×10^4 results from of a typographic error (by one line) and really pertains to the short-period instrument. Similarly, the coupling constants 'μ^2' of 0.8 and 1.0 listed by Charlier & van Gils (1953) for the broadband and short-period systems are probably erroneous since coupling constants for electromagnetic instruments were usually very small (0.05 for the Benioff short-period at Pasadena), and those values (0.8 and 1.0) are actually listed as damping constants H on the microfilmed metadata (Fig. A1b). We thus propose, tentatively, that the constants of the short-period system at Tucson were $T_p = 1$ s; $T_g = 0.24$ s; $\mu^2 = 0.05$; $H_p = 0.8$; $H_g = 1$; $V_{max} = 30\,000$.

In order to verify the value of V_{max}, we compare estimates of body-wave magnitudes m_b which we measured at TUC and PAS for two events occurring in 1946 and 1947 at shorter distances and well recorded at both stations on what amounts to the same instruments, except for a possible difference of magnification. In 1947, and following some experimentation by V.H. Benioff in the 1930s, the magnification at Pasadena had been standardized at $V_{max}^{PAS} = 30\,000$, as documented by operational ledgers at the California Institute of Technology (H. Kanamori, personal communication, 2015), and reported in Charlier & van Gils (1953).

We use the earthquakes of 1946 November 10 and 1947 November 1 in Peru for which we compute magnitudes at Pasadena of $m_b = 7.14$ and 7.19, respectively. Matching these numbers at Tucson would require parameters $V_{max} = 28\,650$ and 48 650, respectively, with a geometrical average of 37 300. Under the circumstances, it seems legitimate to take as V_{max} for the short-period system at Tucson the value of 30 000 listed by Charlier & van Gils (1953) for the broad-band instrument.

(a) **TUCSON Entry in *Charlier and van Gils* [1953]**

Fiche n° Casier: Station : TUCSON

Lat.: 32°14', 8 N. Long.: 110°50',1 W. Altitude: 770 m. Pays : U.S.A.

Temps utilisé : Temps Moyen de Greenwich (signaux horaires scientifiques)

Sous-sol : Caliche et morraine Profondeur: 1 m. Température: Piliers: béton

Enregistrements troublés par microséismes: oui, légèrement.

Constantes :

Type de l'instrument	Composante	Enregistrement	Amortissement	Construction	Marque de temps	Défilement: 1 min.	Sens du mouvement masse	T_g	V_m	T_p	K	μ^2	A_1	l_r	M	V
						mm		s		s					gr.	
Benioff	V	gal	6m	1936	d	30	+	77,0	3.10	1,0		0,80				
					d	60	+	0,236		–		1,0				

(b) **TUCSON Metadata, HSFP, March 1947**

STATION CONSTANTS

Month, year Mar. 1947 *Observer* J.H. Nelson

Lat. 32 ° 15 ' N Long. 110 ° 50 ' W Elev. 770m

INSTRUMENT	COMPONENT	T_o	V_m	DAMPING	U_P*
W-A	N-S	8.0	466	.81	S
W-A	E~~O~~W	8.0	457	.83	E
Benioff	Vert	1.0		.80	Up
SP Galv		.236		1.0	
LP Galv		77		1.0	

* Rapid upward movements of the traces correspond to the ground movements indicated in this column.
The traces progress from {~~left~~} to {~~right~~}. The day's run begins at the {~~top~~} of the gram.

Instrumental constants were last determined on May 1946 (W-A) June 1937 (Benioff)

REMARKS:

Benioff period measured frequently during month.
Adjusted when necessary.

Figure A1. (a) Excerpt from the entry for station Tucson in Charlier & van Gils' (1953) catalogue. Note the magnification listed for the broadband 1–77 system (red arrow), and for the coupling μ^2, both of them probably mistyped. (b) Metadata for station Tucson from the film rolls of the HSFP. Note the more probable interpretation of the parameters 0.8 and 1 in (a) as damping constants (blue arrow). See the text for details.